Single-cell transcriptomics uncover novel role of myeloid cells and T-lymphocytes in Peyronie's disease fibrotic microenvironment

Milenkovic U[1,2], Boeckx B[3,4], Lambrechts D[3,4], Janky R[5], Hatzichristodoulou G[6], van Renterghem K[7], Gevaert T[1], Cellek S[8], Bivalacqua TJ[9], De Ridder D[1,2], Albersen M[1,2]

1. Laboratory of Experimental Urology, Department of Development and Regeneration, KU Leuven

2. Department of Urology, University Hospitals Leuven

3. Laboratory for Translational Genetics, Department of Human Genetics, KU Leuven, Leuven, Belgium
4. VIB Center for Cancer Biology, VIB, Leuven, Belgium

5. VIB Nucleomics Core, VIB, Leuven, Belgium

6. Department of Urology, Martha-Maria Hospital Nuremberg, Germany

7. Jessa Hospital and University of Hasselt, Hasselt, Belgium

8. Faculty of Health, Education, Medicine and Social Care, Medical Technology Centre, Anglia Ruskin University, Chelmsford, UK

9. James Buchanan Brady Urological Institute and Department of Urology, Johns Hopkins School of Medicine, Baltimore, MD, USA

*Corresponding author: Uros Milenkovic, MD, PhD, Department of Urology and Laboratory of Experimental Urology, Catholic University and University Hospitals Leuven, Herestraat 49, 3000 Leuven, Belgium; Email: uros.milenkovic@uzleuven.be

Word count

Abstract: 285; 339 after revisions

Main text: 2490; 2651 after revisions

ABSTRACT

Background: Peyronie's disease (PD) is an acquired fibrotic disease affecting the penile tunica albuginea which can lead to curvature/deformities, shortening and erectile dysfunction. Although immunological mechanisms have been suggested in pathophysiology of PD, these have not been investigated using single-cell transcriptomics.

Objective: To investigate the immunologic signature of plaques from PD patients using immunohistochemistry (IHC) and single cell RNA sequencing (scRNA-Seq).

Design, setting and participants: Surgical samples from 10 PD (≥12 months duration, plaque excision) and 5 controls (plication/penile cancer) were subjected to IHC. An additional 2 PD and 1 control sample were used for ScRNA-Seq (Droplet-based 10xGenomics). Visualization of cell clusters performed using heatmaps and t-SNE plots (BioTuring v2.7.5).

Results: IHC reveals presence of myeloid dendritic cells (DC) (CD68+/TLR4+/CD206+), cytotoxic T-lymphocytes (CD3+/CD8+) and B-lymphocytes (CD20+) in PD plaques, absent in controls. ScRNA-Seq yielded 3312 PD and 5658 control cells. Cell clusters contained fibroblasts (COL1A2+), myofibroblasts (COL1A2+/ACTA2+), smooth muscle (ACTA2+/DES+), endothelial cells (VWF+), myeloid cells (CD14+), T-lymphocytes (CD3D+) and neutrophils(ALPL+). Myeloid cell subclustering showed infiltration of monocyte-derived cells; control tissue contained classical DC and resident macrophages. Lymphocyte subclustering revealed mucosal-associated invariant-T (MAIT) and CTL in PD. Differential gene expression suggests an increased inflammatory and immune response in chronic PD.

Limitations: Relatively limited scRNA-seq sample size (N=3), mitigated by a larger cohort of historic paraffin-embedded samples (N=15), analysed by IHC, which showed largely parallel findings. Due to tissue stiffness and ECM adhesion our PD single cell yield was lower than the control sample.

Conclusions: Our data suggests that even in chronic stage (painless/stable curvature) there is a sustained inflammatory reaction. While there is an increased amount of vascularisation and collagen production, the inflammation is driven by specialized monocyte-derived, CTL and MAIT cells. These findings could uncover new avenues in the medical treatment of PD.

Patient summary: In this report, we looked at the role of the immune system in patients suffering from Peyronie's disease. We found that, even though in a stabilised, chronic disease stage, there is activation of both innate and adaptive immune systems, implicating potential for novel treatments.

INTRODUCTION

Peyronie's disease (PD) is a fibrotic disorder characterised by penile scarring resulting in irreversible penile curvature, currently remaining an incurable and sexually debilitating condition. It results from chronic fibrosis of the tunica albuginea (TA), a connective tissue sheath surrounding the corpora cavernosa. This TA fibrosis leads to asymmetrical stretching of the CC during erection. The prevalence of PD has been suggested to be 0.4-9% in the general population, while also associated with difficult-to-treat erectile dysfunction (ED)[1,2] and psychological stress/depression[3,4]. Contemporary recommended treatment options include surgical correction of the penile curvature/deformity or local injection of collagenase[5]. However, long-term results remain relatively unsatisfactory and can only partly improve the curvature, without tackling the underlying molecular biology. The most widely accepted hypothesis postulates that PD is caused by repetitive trauma to the erect penis during intercourse[6-9]. In this model, mechanical stress activates transforming growth factor-β1 (TGF-β1) (stored in the extracellular matrix (ECM)) which subsequently stimulates fibroblast-to-myofibroblast (MFB) transformation[10-12]. Myofibroblasts are thought to be the hallmark of PD due to their unique capacity to produce large quantities of ECM and incite tissue contraction. There is a severe lack in conservative/medical FDA-/EMA-approved therapeutics due to the poor understanding of the precise underlying pathophysiological processes leading to PD, despite extensive research into myofibroblast biology[13]. The immune system has been implicated in PD fibrosis. Ralph et al.[14] analysed acute phase PD-plaques 20 years ago, revealing a role for macrophages and T-lymphocytes. Moreover, Magee et al.[15] characterised gene expression in PD patients using microarrays, showing upregulation of general pro-inflammatory genes such as pleiotrophin, MCP-1, and early growth response protein. Despite these findings, direct analysis and characterisation of immune cell content and pathways of chronic plaques have not been performed.

In the acute stage of PD, there is a clear inflammatory phase, with symptoms such as pain and worsening curvature. In the chronic stage however, the disease seems to subside with stabilising curvature and disappearance of local discomfort. At this point, it is considered irreversible and (surgical) treatment can be commenced. We hypothesized that this acute inflammation might persist into the chronic phase and perpetuate the contained, pro-fibrotic PD micro-environment.

Since myofibroblasts are ubiquitous in normal wound healing and notoriously difficult to target, we wanted to achieve a better insight into genes and pathways that govern the chronic, seemingly "quiescent" PD immunological landscape. In this study, we have performed in-depth comparison of PD and controls using immunohistochemistry and single-cell sequencing

(scRNA-Seq) in order to map the cellular and transcriptomic landscape of the disease, with a focus on immunological aspects.

MATERIALS AND METHODS

Biopsies from TA were obtained from patients undergoing surgery for either PD (N=12) or penile surgery for different reasons (control, N=6). Inclusion criteria for tissue harvesting in PD patients were 1) stable/chronic disease stage (≥ 12 months duration), 2) no previous penile surgery or intralesional injection therapy and 3) plaque excision followed by grafting as the surgical procedure. Control patient tissue was healthy TA excised during either congenital curvature repair (plication) or penile cancer surgery.

Plaque tissue was carefully dissected (in case of PD), removal of adjacent cavernosal tissue was ensured and samples were suspended in formaldehyde for IHC (N=15) or fresh culture medium for scRNA-Seq (N=3). This study has been approved by the local ethical committee and biobank (projects s59964 and s60624).

Immunochemistry

To assess morphology and immune cell presence; we performed hematoxylin-eosin (H&E), IHC and immunofluorescence (IF) staining on paraffin-embedded patient PD and control samples. Imaging was performed by DM2000 microscope (Leica, Germany). For IHC, samples were auto-stained with BOND-MAX (Leica, Germany). Tris/EDTA (pH 9) was used for epitope retrieval and treated for 30min with ready-to-use mouse monoclonal anti-CD68 (IR60961-2), CD3 (IR50361-2), CD56 (IR62861-2), CD15 (IR06261-2), CD20 (IR60461-2), CD138 (IR64261-2), CD4 (IR64961-2), CD8 (IR62361-2, Agilent, US). Detection was performed by the BOND polymer detection kit (Leica, Germany).

Semi-quantitative scoring for H&E staining was performed based on (i) the thickness of TA (1-1.5-2-2.5-3), (ii) vascular structures (0-present/1-absent), (iii) inflammatory infiltrate (0-present/1-absent) and (iv) cartilage formation/calcification (0-present/1-absent), adapted from a previous report and all scorings were summed and represented as mean values (±SD)[4,16].

Regarding IF; after deparaffinisation, sections were incubated with 1% BSA and PBS for 2h and overnight 4°C with mouse monoclonal anti-TLR4 antibody (ab22048, 1:100, Abcam, UK) and rabbit polyclonal anti-CD206 (ab64693, 1:100). Incubation for 2h with donkey anti-mouse secondary antibody conjugated with Cy3-fluorescein (AB_2340813, 1:400) and donkey anti-rabbit secondary antibody conjugated with Cy5-fluorescein (AB_2340607, 1:500, Jackson ImmunoResearch, UK). DAPI nuclear staining and SlowFade fixation (ThermoFisher, US).

Imaging was performed using a Nikon Eclipse C1-microscope with NIS elements (v4.60). Optical density was quantified using ImageJ (v1.8) and expressed as ratios compared to DAPI. Statistical analysis using a Student's t-test was performed using Graphpad (v8.0). P-value <0.05 was considered statistically significant.

ScRNA sequencing

On laboratory arrival, samples (PD, N=2 and control, N=1) were rinsed and PD samples were macroscopically examined for fibrosis localisation. Precise preparation of the single-cell suspension described under supplementary methods.

Raw gene expression matrices generated using CellRanger (v2.0.0) were converted to a Seurat-object using the Seurat R-package. Gene expression matrices were normalized to total cellular and mitochondrial read count using linear regression (Seurat RegressOut). To reduce dimensionality, resulting variably expressed genes were summarized by principle component analysis (PCA), and first 19 components visualized using tSNE dimensionality reduction (resolution 0.8). Cell clusters were annotated to known biological cell types using canonical marker genes and BioTuring software (v2.7.5). Gene expression of individual genes was visualised by box plots. Fold changes between cell types were calculated using student's t-Test (Graphpad v8.0). Sub-clustering of myeloid cells and lymphocytes was performed through a combination of unsupervised clustering (Bioturing software) and manual curation, described under supplementary methods.

RESULTS

H&E from control TA samples showed uniform vascular structures from adjacent vascular plexus with low cellularity (diamond, Fig. 1C) and organized collagen fibres. PD plaques were characterised by increased thickness of TA, decreased vascular protrusions and increased inflammatory infiltrate. Inflammatory cells were found mostly in the perivascular area of the TA containing disorganized collagen fibres and lymphoid aggregates. Moreover, cartilage formation/calcification was visible in 2/10 PD samples (Figure 1A-B).

IHC shows abundance of CD68+ in PD, while only scarcely present in controls (Fig 2A-C). Subsequent immunofluorescence (co)staining with CD206/MRC1 and Toll-Like receptor 4 (TLR4) indicate the presence of myeloid dendritic cells (DC) in PD (Fig. 2E-H). DC were present in close contact with CD3+ T-lymphocytes (Fig. 3A-C) and CD20+ B-lymphocytes (Fig. 4A-C) in lymphoid aggregates. T-lymphocytes were identified as predominantly cytotoxic T-lymphocytes (CTL) (CD8+), with weak positive staining for T-helper (CD4+) cells (Fig. 3E-

K). PD and control plaques were negative for plasma cell marker CD138, granulocyte marker CD15 and NK cell marker CD56 (Fig. 4D-M).

Further, single-cell RNA sequencing (scRNA-Seq) identified 5658 and 3312 cells in control and PD respectively. Figure 5 shows combined tSNE-plot visualization. Cells were initially divided into 15 clusters, after which clusters were curated and annotated (Fig. 5A). Figure 5B shows the heatmap for expression of marker genes. Six genes were then visualised in pseudo-coloured tSNE-plots and boxplots indicating the relative fold change per cluster (Fig. 5C). We were able to identify distinct cell clusters containing predominantly fibroblasts (THY1/LUM/COL1A1/COL3A1/MMP2/FBLN1/DCN), MFB (fibroblast markers + ACTA2/TAGLN/STEAP4/TM4SF1/IGFBP5), smooth muscle cells (SMC) (ACTA2/TAGLN/IGFBP5/DES/FRZB/RERGL/MYH11), endothelial cells (EC) (VWF/CD34/PECAM1/ACKR1/CLEC14A/IFI27/CLDN5), myeloid cells (CD14/MRC1/CD163), T-lymphocytes (CD3D/TRAC) and neutrophils (ALPL, GCA).

Our data shows a 1.6-fold increase ($p<0.05$) in SMC, 3.2-fold increase ($p<0.05$) in MFB, 1.3-fold increase in myeloid cells ($p<0.0001$) and 4.1-fold increase in lymphocytes ($p<0.01$) compared to control tissue (Fig. 5D-E). Moreover, no statistically significant difference was found in endothelial cells together with a 50% decrease ($p=0.03$) in FBs in PD versus control. Interestingly, there was a neutrophil depletion in the PD samples, i.e. 43 cell cluster solely present in control. However, considering the low cell and transcript number, these will not be discussed further to avoid biased interpretation.

Myeloid cell subsets

Further differentiation of the myeloid cell cluster revealed presence of distinct subclusters expressing genes which are 1) monocyte-associated (CD14/FCN1/S100A9/LYZ/VCAN/CD45), 2) monocyte- (CD14/CD16/FCN1) and macrophage-related (STAB1/SEPP1/TYROBP/C1QA/FOLR2) (=monocyte-derived macrophage-like), 3) monocyte-associated and related to DC-activation (FCER1A/CD1C/CLEC10A) (=monocyte-derived DC-like), 4) DC and macrophage-related (=classical dendritic cell type 2 (cDC2)) (MAFB/ZEB2/KLF4/MRC1/CD11b/SIRPA/CD93/CD81/CD4 + F13A/SEPP1/STAB1/TYROBP/AIF1/C1QA/FOLR2) and 5) resident macrophages (M2-like phenotype) (F13A/SEPP1/TYROBP/AIF1/C1QA/FOLR2) (Fig. 6A-C). While control tissue contains predominantly cDC2 and resident macrophages (47% and 44.5% of control myeloid cells resp.), PD samples show a high number of infiltrating monocyte-derived cells (73% of myeloid cells) (Fig. 6B).

Differential gene expression between PD and control myeloid cells are shown in supplementary tables 1-2 with volcano plot and heatmap visualization in Fig. 6E-F. Upregulated genes in PD include HLA-B (antigen-presentation), FCER1A (immune/inflammatory response), PFN1 (Wnt—pathway), LSP1 (cellular defense), THSB10 (cellular migration). Downregulated genes include FBLN1 (ECM-adhesion), STAB1 (cell-adhesion), MRC1 (endocytosis), CFD (Notch-pathway), DAB (Wnt-pathway inhibition), CCL4L2/CCL2 (ECM-remodelling, inflammation, chemotaxis) and TIMP2 (anti-inflammatory).

Lymphoid cell subsets

In-depth characterization of lymphocytes showed presence of T-lymphocytes (TRAC/CD3D/CD3E) (Fig. 6A-C), with a limited number of B-lymphocytes (CD79a), NK cells (XCL1/TNFRSF18) and basophils (FCER1A) (data not shown). T-lymphocytes could be subdivided into 1) conventional CD8+ T-effector cells (cytotoxic, GZMA/GZMK/GZMM/CCL4/CCL5/CXCR3/CD45 positive, CD62L/CCR7 negative), 2) CD4+ T-helper cells (low cell number) and 3) mucosal-associated invariant T- (MAIT) cells (KLRB1/IL7R/CCR6/CXCR6) (Fig. 6B-C).

Differential gene expression between PD and control are shown in supplementary tables 3-4. Volcano plot and heatmap visualization in Fig. 7E-F. Genes upregulated in PD include ACKR1/CCL5 (inflammatory response), CD74 (immune response), PFN1 (Wnt-pathway), HLA-A (antigen-presentation), GZMK (proteolysis) and FXYD5 (cellular migration). Among downregulated genes observed in PD were IL7R/TNF/TGFB1/s100A4 (immune response, ECM-remodelling), BAX/BCL2 (apoptosis), PHPT1 (T-cell signalling attenuation), LCP1 (ECM-adhesion), STK4 (Wnt-signalling inhibition) and ITGB2 (cell-adhesion).

DISCUSSION

To our knowledge, this is the first report examining chronic Peyronie's disease fibrotic plaques and TA control samples using novel sequencing approaches.

Due to the complexity of inflammatory responses in fibrotic diseases, a profound grasp of cell populations and mediators is needed to elucidate tissue specific differences and optimizing treatment. Clinical trials shed light on these variances, where administering broad "anti-inflammatory" drugs appears insufficient. In PD, injection of corticosteroids failed to demonstrate clinical benefit; clinical trials with corticosteroids or anti-TNF in pulmonary fibrosis (PF) did not show improvement and combination of azathioprine/prednisone even worsened outcomes[17,18]. Moreover, gene expression studies in systemic sclerosis (SSc) cohorts have

led to the identification of intrinsic subsets; inflammatory, fibroproliferative, limited and normal-like. The same is true for PF, where patients can be subdivided in at least 2 subtypes[19]. Unsurprisingly, these subsets respond differently to therapy[19].

Screening of 10 PD and 5 control plaques using IHC suggests co-occurrence of DC, cytotoxic T-lymphocytes and B-lymphocytes in lymphoid aggregates. To investigate this hypothesis further, we performed scRNA-seq. This showed an increased presence of MFB and SMC, which suggests ongoing fibrosis-related ECM-production (Fig. 5). Moreover, our findings suggest interplay of innate and acquired/adaptive immune system in chronic PD. The immunological involvement in fibrosis is complex and dependent on inflammatory stage and tissue type. Initial injury in PD is thought to be repetitive microtrauma during intercourse[20], similar to SSc and PF where microvascular and epithelial damage are considered the primary injury[21,22]. Regarding innate immunity; monocytes, macrophages (Mac) and dendritic cells (DC) contain a staggering amount of plasticity responding to a variety of stimuli. These include endogenous "danger"-molecules, recognized by TLRs (= innate immune system stress sensors)[23,24]. Initial inflammation occurs through inflammatory "M1"-cells, replaced by fibrotic "M2" myeloid cells (in normal circumstances reparative/resolving). Although this paradigm oversimplifies their actual highly dynamic range, it does illustrate distinct phenotypes in different stages of the fibrotic process.

Nomenclature is mainly based on their origin, e.g. resident macrophages are mainly yolk sac/embryonally-derived and have a capacity for self-renewal, while DCs can either be derived from common bone marrow progenitors or monocyte-derived (inflammation-related settings). However, despite their initial phenotype, experimental data shows their capacity for becoming more *monocyte-*, *DC-* or *Mac-like* in certain situations[23]. Our data showed an increased influx of "inflammatory" monocyte-derived cells "*M1 cells*" into the PD plaque (Fig. 6)[25,26]. Co-expression of CD1c/FCER1A/MRC1 suggests DC differentiation ("*DC-like*"); their function in includes secretion of IL-1/TNF/IL-12 and activation of CD4/CD8+ T-lymphocytes[23,27–29]. Phenotypes with expression of CD16/CD163 and F13A (and lacking DC-markers) are usually described as *Mac-like*, with phagocytosis and antigen-presentation being their hallmark. Myeloid cell differential gene expression (Fig. 6E-F) shows an upregulated inflammatory cascade in PD (Fig. 6F/suppl. table 1).

Conversely, control patient myeloid cells mainly contain DCs and resident macrophages (M2-phenotype). DCs can be subdivided into plasmacytoid DC, 'classical' DC type 1 and 2 (cDC1-cDC2) based on expression of key transcription factors IRF8/IRF4[23,30]. The majority of DC present in human blood, tissue and lymphoid organs can be classified as cDC2 and lie on a 'spectrum' where subpopulations are "*monocyte-like*" or "*DC-like*" depending on transcriptomic

signature (Fig. 6A)[31,32]. Myeloid cDC2 strongly express lectins/TLRs, thus being the first defence against damage and first-responders against microtrauma in the TA. The gene signature in control tissue pertains to tissue homeostasis (e.g. ECM/cell-adhesion, endocytosis, ECM-remodelling) (Fig. 6E-F).

In a second finding, T-lymphocytes appear to play a significant role as well. IHC shows mostly CD8+ CTL (Fig. 3) with also a significant enrichment in scRNA-seq (4-fold increase in T-lymphocytes) compared to control (Fig. 5E). Further characterisation shows that an important subset (PD + control) expresses hallmark genes for non-conventional MAIT cells (KLRB1/IL7R /CCR6/CXCR6)[32]. Traditionally, T-/B-lymphocytes belong to the adaptive immune system, mounting a long-term response against injuries, whereas the innate immune system recognises pathogens immediately and incites an adaptive response. MAITs are innate-like T-cells with an CTL effector-memory phenotype, naturally occurring throughout the body and able to produce pro-inflammatory cytokines (e.g. IL-17/granzymes/IFN-γ/TNF) and myofibroblast transformation upon activation by MHC class I molecules (MR1)[32].

Our data shows the presence of T-effectors (30%, 29/96) and MAIT-cells (60%, 58/96) in PD, while control T-lymphocytes mainly consist of MAITs (80%, 32/40). Differential gene expression (Fig. 7E-F) in PD shows an increased cellular migration, inflammatory response and cytotoxicity (e.g. GZMK) in PD. However, even in controls, they are immunologically active expressing chemo/cytokines such as IL7R/TNF/NCR3/PRF1/OSTF1/TGF-β1, underlying their role as gatekeepers both in healthy and fibrotic tissue. MAITs are a relatively recent finding and are increasingly recognized in auto-immune and fibrotic disease such as inflammatory bowel disease, and cirrhosis[32]. This is the first report to describe the presence of MAIT cells in penile tissue.

Interestingly, B-lymphocytes characterised in IHC were not found in the scRNA-seq analysis. This could mean that there are indeed subtypes of PD with a slightly different inflammatory constitution and that medical treatment needs to be patient-tailored. Our scRNA-seq sample size is limited due to difficult availability of fresh PD and control tissue; we tried to overcome this by analysing paraffin-embedded TA, which generally parallel findings. Moreover, lower single cell suspension yield in PD can be explained by the higher tissue stiffness and adhesion to the ECM.

Nonetheless, here we showed that chronic PD plaques are still highly immunologically active, despite disappearance of meaningful clinical deterioration (stabilised curvature) and pain. Our goal was to demonstrate the single cell landscape of fibrosis to identify potential drivers of PD plaque formation, an undertaking that may also catalyse biological discoveries with immediate therapeutic relevance.

Future experiments could focus on temporal difference in disease progression (early “stabilised”/chronic vs late) and differentiate between patients who had received topical or

intra-lesional therapy (no scRNA-seq patients had received previous therapy). Moreover, novel software appliances (e.g. ConnectivityMap from the Broad Institute, http://clue.io) can integrate and process publicly available sequencing data in order to record the changes in cellular signatures and transcriptional regulation in response to chemical and genetic perturbation. In this way, gene expression profiling technology can connect genes, drugs and disease states by virtue of common expression profiles, thus possibly uncovering novel applications for readily available and well-known small molecules.

CONCLUSION

Our data suggests that even in the chronic stage (painless/stable curvature) there is a sustained inflammatory reaction. While there is an increased amount of vascularisation and collagen production, the inflammation is driven by specialized monocyte-derived, cytotoxic T-lymphocytes and mucosal-associated invariant T-cells. These findings could uncover new avenues in the medical treatment of PD.

ACKNOWLEDGEMENTS

The authors would like to thank Thomas Van Den Broeck (MD, PhD) and Marcus Ilg (PhD) for their excellent help, attention to detail and critical thinking, providing invaluable input for this manuscript.

The authors would also like to thank Thomas Steelandt (MD) of the pathology department for their input and help in analysing the histopathological sections.

This research has been funded by the Fund for Peyronie's Disease Research, European Society for Sexual Medicine (ESSM) and the Fund for Translational Biomedical Research (FTBR) ("Klinische onderzoeks- en opleidingsraad" (KOOR)) of KU/UZ Leuven

CONFLICTS OF INTEREST

The authors have no conflicts of interest to disclose

SUPPLEMENTARY METHODS

Single-cell suspension

Each sample was manually shredded on ice to 1mm^3 pieces (removing any residual cavernosal tissue) and placed onto 10 ml digestion medium (0.2% collagenase I/II

(ThermoFisher Scientific), DNAse I (Sigma) and 25 units dispase (Invitrogen) in DMEM (ThermoFisher Scientific). Incubation occurred for 15min at 37°C and manual disruption every 5 min. Subsequently, the samples were vortexed (10s) and pipetted up and down for using pipettes of descending sizes (25 ml, 10 ml and 5 ml). Next, we added 30 ml ice-cold PBS (neutral pH) (ThermoFisher Scientific) with 2% FBS (ThermoFisher Scientific) and filtered using a 40-μm nylon sieve (ThermoFisher Scientific). After centrifugation at 120g during 5 min (4°C), the supernatant was removed. The remaining cell pellet was resuspended in 2 mL red blood cell lysis buffer and carried over into a 2-mL DNA low bind tube. Samples were again centrifuged (120g, 4°C, 5 min) after a 5 min room temperature incubation. Samples were next resuspended in 1 ml PBS containing 8 μl UltraPure BSA (50 mg ml−1; AM2616, ThermoFisher Scientific) and filtered over Scienceware Flowmi 40-μm cell strainers (VWR) using wide-bore 1 ml low-retention filter tips (Mettler-Toledo). Finally, 10 μl cell suspension was counted using an automated cell counter (Luna) to determine the concentration of live cells. Throughout the dissociation procedure, cells were maintained on ice whenever possible, and the entire procedure was completed in less than 1 h (typically ~45 min) to avoid dissociation-associated artefacts.

Droplet-based scRNA-seq

Single-cell suspensions were converted to barcoded scRNA-seq libraries by using the Chromium Single Cell 3' Library, Gel Bead & Multiplex Kit and Chip Kit (10x Genomics), aiming for an estimated 4,000 cells per library and following the manufacturer's instructions. Samples were processed using kits pertaining to either the V1 or V2 barcoding chemistry of 10x Genomics. Single samples are always processed in a single well of a PCR plate, allowing all cells from a sample to be treated with the same master mix and in the same reaction vessel. For each patient, all samples (Peyronie's disease and control) were processed in parallel in the same thermal cycler. Libraries were sequenced on an Illumina HiSeq4000, and mapped to the human genome (build hg19) using CellRanger (10x Genomics). Gene positions were annotated as per Ensembl build 85 and filtered for biotype (only protein-coding, long intergenic non-coding RNA, antisense, immunoglobulin or T-cell receptor).

Single-cell gene expression quantification and determination of the major cell types

Raw gene expression matrices generated per sample using CellRanger (version 2.0.0) were combined in R (version 3.3.2), and converted to a Seurat object using the Seurat R package (version 1.4.0.7). From this, all cells were removed that had either fewer than 201 UMIs, over 6,000 or below 101 expressed genes, or over 10% UMIs derived from mitochondrial genome. From the remaining 8970 cells, gene expression matrices were normalized to total cellular

read count and to mitochondrial read count using linear regression as implemented in Seurat's RegressOut function. As a result, none of the principle components subsequently identified were correlated with transcript count (data not shown). From the remaining 8970 cells, variably expressed genes were selected as having a normalized expression between 0.125 and 3, and a quantile-normalized variance exceeding 0.5. To reduce dimensionality of this dataset, the resulting variably expressed genes were summarized by principle component analysis, and the first 19 principle components further summarized using tSNE dimensionality reduction using the default settings of the RunTSNE function. Cell clusters in the resulting two-dimensional representation were annotated to known biological cell types using canonical marker genes and BioTuring browser v2.2.

REFERENCES

1. Al-Thakafi, S. & Al-Hathal, N. Peyronie's disease: A literature review on epidemiology, genetics, pathophysiology, diagnosis and work-up. *Translational Andrology and Urology* vol. 5 280–289 (2016).

2. Nelson, C. J. *et al.* The chronology of depression and distress in men with peyronie's disease. *Journal of Sexual Medicine* **5**, 1985–1990 (2008).

3. Hatzichristodoulou, G., Osmonov, D., Kübler, H., Hellstrom, W. J. G. & Yafi, F. A. Contemporary Review of Grafting Techniques for the Surgical Treatment of Peyronie's Disease. *Sexual Medicine Reviews* vol. 5 544–552 (2017).

4. Russo, G. I. *et al.* Clinical Efficacy of Injection and Mechanical Therapy for Peyronie's Disease: A Systematic Review of the Literature[Figure presented]. *European Urology* **74**, 767–781 (2018).

5. Devine, C. J., Somers, K. D., Jordan, G. H. & Schlossberg, S. M. Proposal: Trauma as the cause of the Peyronie's lesion. in *Journal of Urology* vol. 157 285–290 (Elsevier Inc., 1997).

6. Milenkovic, U. *et al.* Simvastatin and the Rho-kinase inhibitor Y-27632 prevent myofibroblast transformation in Peyronie's disease-derived fibroblasts via inhibition of YAP/TAZ nuclear translocation. *BJU International* **123**, 703–715 (2019).

7. Milenkovic, U., Ilg, M. M., Cellek, S. & Albersen, M. Pathophysiology and Future Therapeutic Perspectives for Resolving Fibrosis in Peyronie's Disease. *Sexual Medicine Reviews* vol. 7 679–689 (2019).

8. Ilg, M. M. *et al.* Antifibrotic Synergy Between Phosphodiesterase Type 5 Inhibitors and Selective Oestrogen Receptor Modulators in Peyronie's Disease Models. *European Urology* **75**, 329–340 (2019).

9. Gonzalez-Cadavid, N. F. & Rajfer, J. Mechanisms of disease: New insights into the cellular and molecular pathology of Peyronie's disease. *Nature Clinical Practice Urology* vol. 2 291–297 (2005).

10. Milenkovic, U., Albersen, M. & Castiglione, F. The mechanisms and potential of stem cell therapy for penile fibrosis. *Nature Reviews Urology* **16**, 79–97 (2019).

11. Hinz, B. & Lagares, D. Evasion of apoptosis by myofibroblasts: a hallmark of fibrotic diseases. *Nature Reviews Rheumatology* vol. 16 11–31 (2020).

12. Hinz, B. *et al.* The myofibroblast: One function, multiple origins. *American Journal of Pathology* **170**, 1807–1816 (2007).

13. Davis, C. J. The microscopic pathology of Peyronie's disease. *Journal of Urology* **157**, 282–284 (1997).

14. Ralph, D. J., Mirakian, R., Pryor, J. P. & Bottazzo, G. F. The immunological features of Peyronie's disease. *Journal of Urology* **155**, 159–162 (1996).

15. Magee, T. R. *et al.* Gene expression profiles in the Peyronie's disease plaque. *Urology* **59**, 451–457 (2002).

16. Raghu, G. *et al.* Treatment of idiopathic pulmonary fibrosis with etanercept: An exploratory, placebo-controlled trial. *American Journal of Respiratory and Critical Care Medicine* **178**, 948–955 (2008).

17. Assassi, S. *et al.* Dissecting the heterogeneity of skin gene expression patterns in systemic sclerosis. *Arthritis and Rheumatology* **67**, 3016–3026 (2015).

18. Yang, I. v. *et al.* Expression of cilium-associated genes defines novel molecular subtypes of idiopathic pulmonary fibrosis. *Thorax* **68**, 1114–1121 (2013).

19. Pendergrass, S. A. *et al.* Limited Systemic Sclerosis Patients with Pulmonary Arterial Hypertension Show Biomarkers of Inflammation and Vascular Injury. *PLoS ONE* **5**, e12106 (2010).

20. Distler, J. H. W. *et al.* Shared and distinct mechanisms of fibrosis. *Nature Reviews Rheumatology* **15**, 705–730 (2019).

21. Land, W. G. The role of damage-associated molecular patterns (DAMPs) in human diseases part II: DAMPs as diagnostics, prognostics and therapeutics in clinical medicine. *Sultan Qaboos University Medical Journal* vol. 15 e157–e170 (2015).

22. Kapellos, T. S. *et al.* Human monocyte subsets and phenotypes in major chronic inflammatory diseases. *Frontiers in Immunology* vol. 10 (2019).

23. Collin, M. & Bigley, V. Human dendritic cell subsets: an update. *Immunology* vol. 154 3–20 (2018).

24. Tang-Huau, T. L. *et al.* Human in vivo-generated monocyte-derived dendritic cells and macrophages cross-present antigens through a vacuolar pathway. *Nature Communications* **9**, 1–12 (2018).

25. Zaba, L. C. *et al.* Psoriasis is characterized by accumulation of immunostimulatory and Th1/Th17 cell-polarizing myeloid dendritic cells. *The Journal of investigative dermatology* **129**, 79–88 (2009).

26. Liao, C. te *et al.* Peritoneal macrophage heterogeneity is associated with different peritoneal dialysis outcomes. *Kidney International* **91**, 1088–1103 (2017).

27. Castell-Rodríguez, A., Piñón-Zárate, G., Herrera-Enríquez, M., Jarquín-Yáñez, K. & Medina-Solares, I. Dendritic Cells: Location, Function, and Clinical Implications. in *Biology of Myelomonocytic Cells* (InTech, 2017). doi:10.5772/intechopen.68352.

28. Ferenbach, D. & Hughes, J. Macrophages and dendritic cells: What is the difference? *Kidney International* **74**, 5–7 (2008).

29. Guilliams, M. *et al.* Dendritic cells, monocytes and macrophages: A unified nomenclature based on ontogeny. *Nature Reviews Immunology* vol. 14 571–578 (2014).

30. Tang-Huau, T. L. *et al.* Human in vivo-generated monocyte-derived dendritic cells and macrophages cross-present antigens through a vacuolar pathway. *Nature Communications* **9**, (2018).

31. Park, D. *et al.* Differences in the molecular signatures of mucosal-associated invariant T cells and conventional T cells. *Scientific Reports* **9**, (2019).

32. Toubal, A., Nel, I., Lotersztajn, S. & Lehuen, A. Mucosal-associated invariant T cells and disease. *Nature Reviews Immunology* **19**, 643–657 (2019).

Figure 1

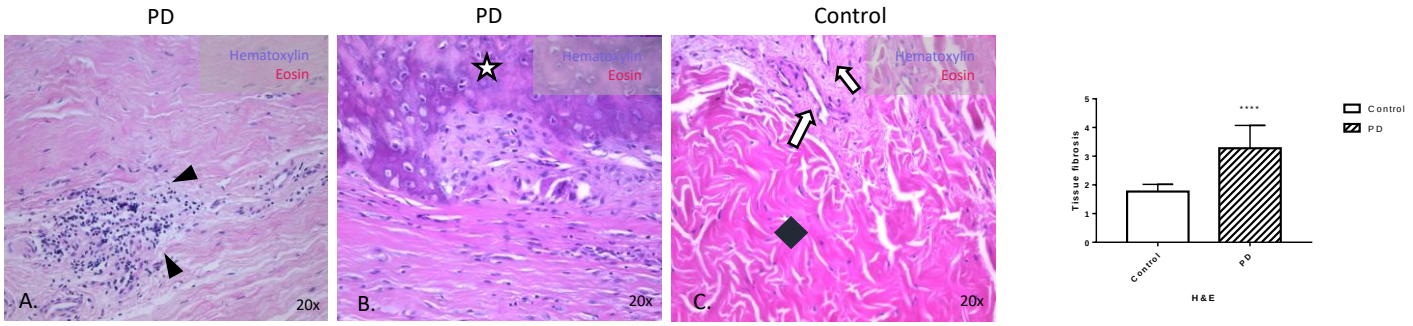

Figure 2

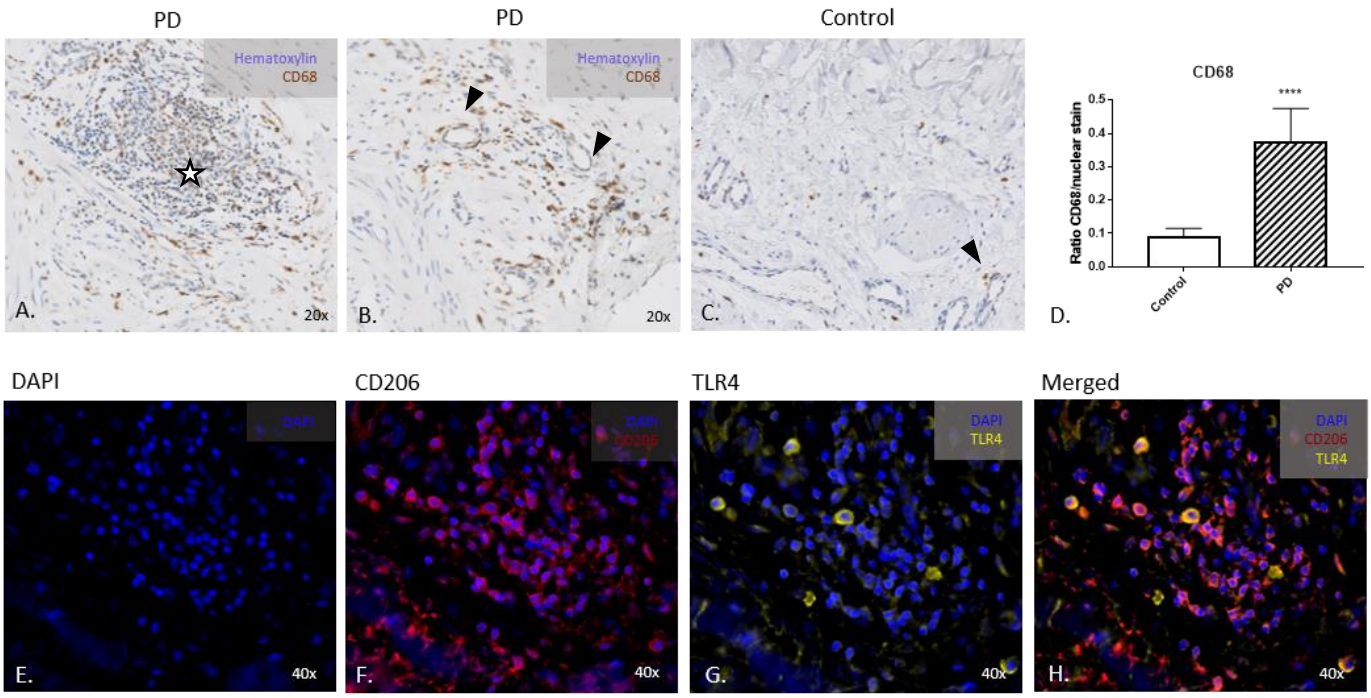

Fig. 1 Hematoxylin-eosin staining of control TA samples (N=5) versus Peyronie's disease samples (N=10). *Control TA samples (Fig. 1C) uniformly have vascular structures (arrows) from the adjacent vascular plexus with low cellularity (diamond) and organized collagen fibers. PD samples have calcifications (star) (Fig. 1A-B) and dense inflammatory infiltrate peri-vascularly with organized deposition of collagen fibers (triangle) (Fig. 1B).*

Fig. 2 Immunohistochemical staining in control versus Peyronie's disease patients. *Immunohistochemical staining for CD68, a commonly used macrophage marker. Control TA samples only contained a limited number of resident macrophages (N=5) (Fig. 2C). In PD patients, macrophages are significantly prevalent in the peri-vascular area of the tunica albuginea (TA), on the border of the TA and its vascular plexus and in lymphoid aggregates (N=10) (Fig. 2A-B).*
Co-staining of CD 206 and TLR4 reveals a co-localization of both proteins in these aggregates (Fig. 2E-H)

Figure 3

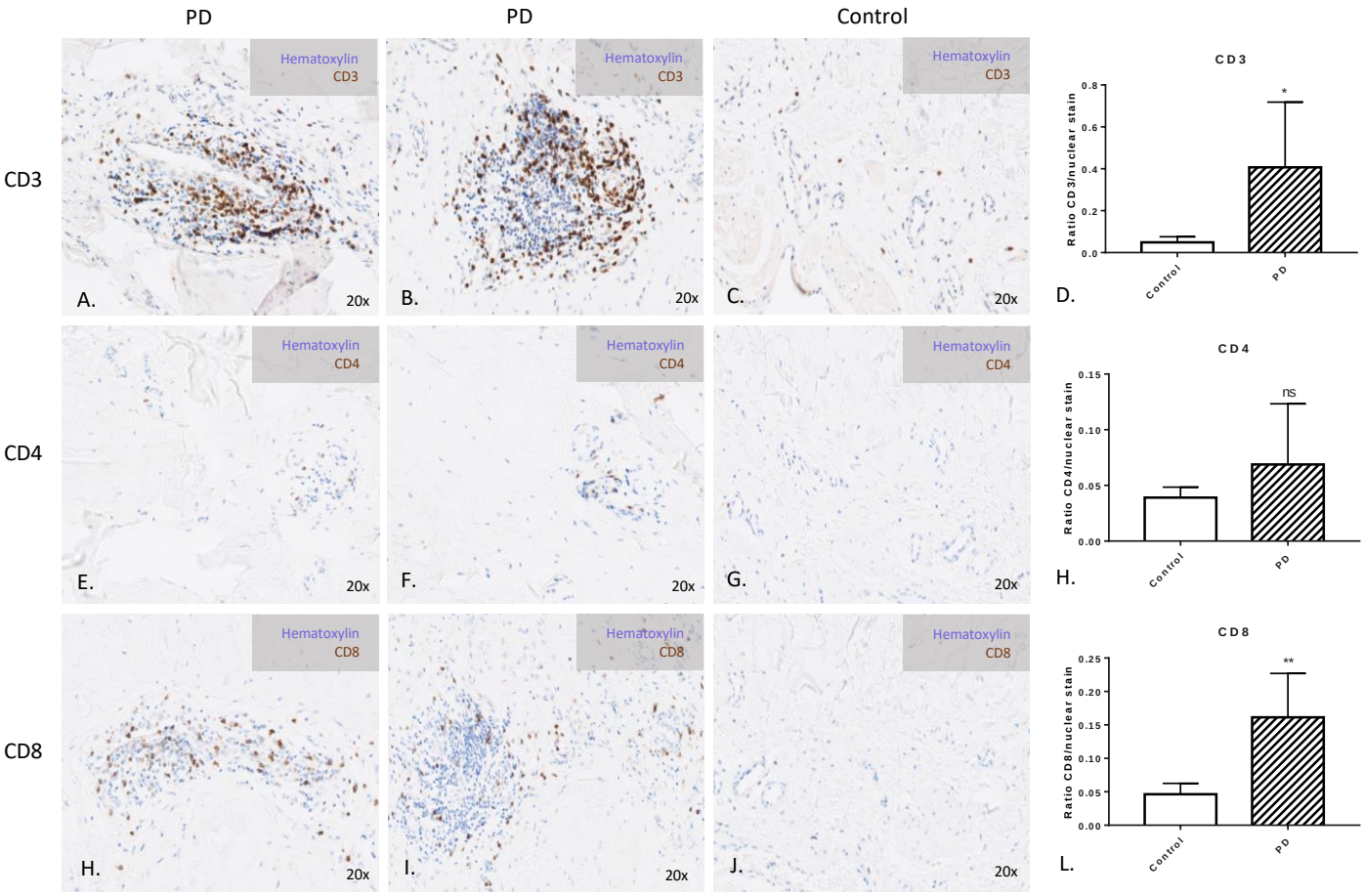

Fig. 3 Immunohistochemical staining for CD3, CD4 and CD8, a commonly used T-lymphocyte marker. *Control TA samples only contained a limited number of TL (N=5) (Fig. 3C, G and K). CD3+/CD8+ TL (marker for cytotoxic T-lymphocytes) were more abundant than CD3+/CD4+ (marker for T-helper cells) ones. TL co-localized with MΦ/DC and BL in lymphoid aggregates. Optical density was quantified using ImageJ software (v1.8) and expressed as a ratio in comparison to the nuclear stain (hematoxylin).*

Figure 4

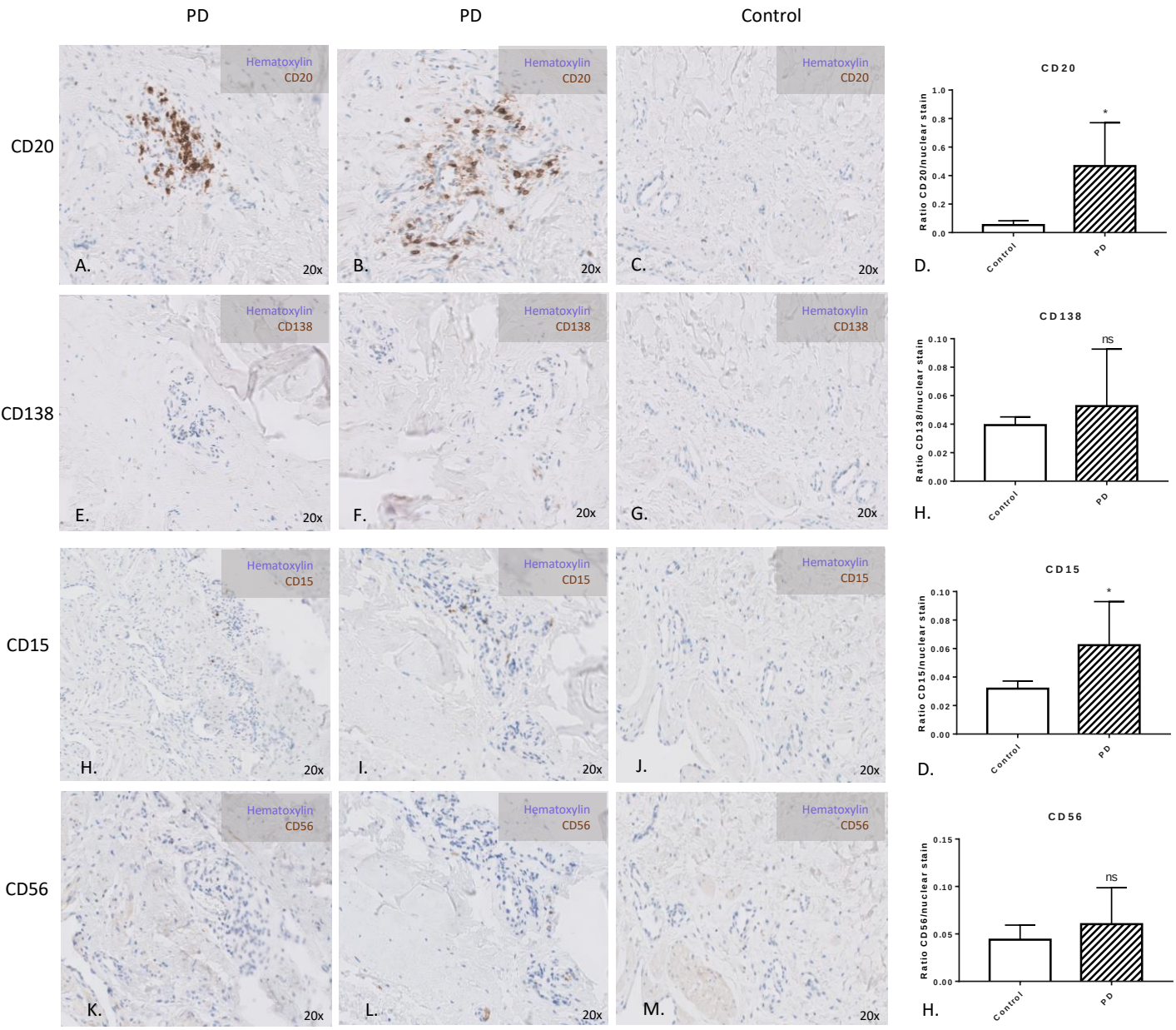

Fig. 4 Immunohistochemical staining for CD20 (B-lymphocyte marker), CD138 (plasma cell marker), CD15 (granulocyte marker) and CD56 (natural killer cell marker). *Both control TA (N=5) and PD (N=10) samples lacked an expression of CD20, CD138, CD15 and CD56. Optical density was quantified using ImageJ software (v1.8) and expressed as a ratio in comparison to the nuclear stain (hematoxylin).*

Figure 5

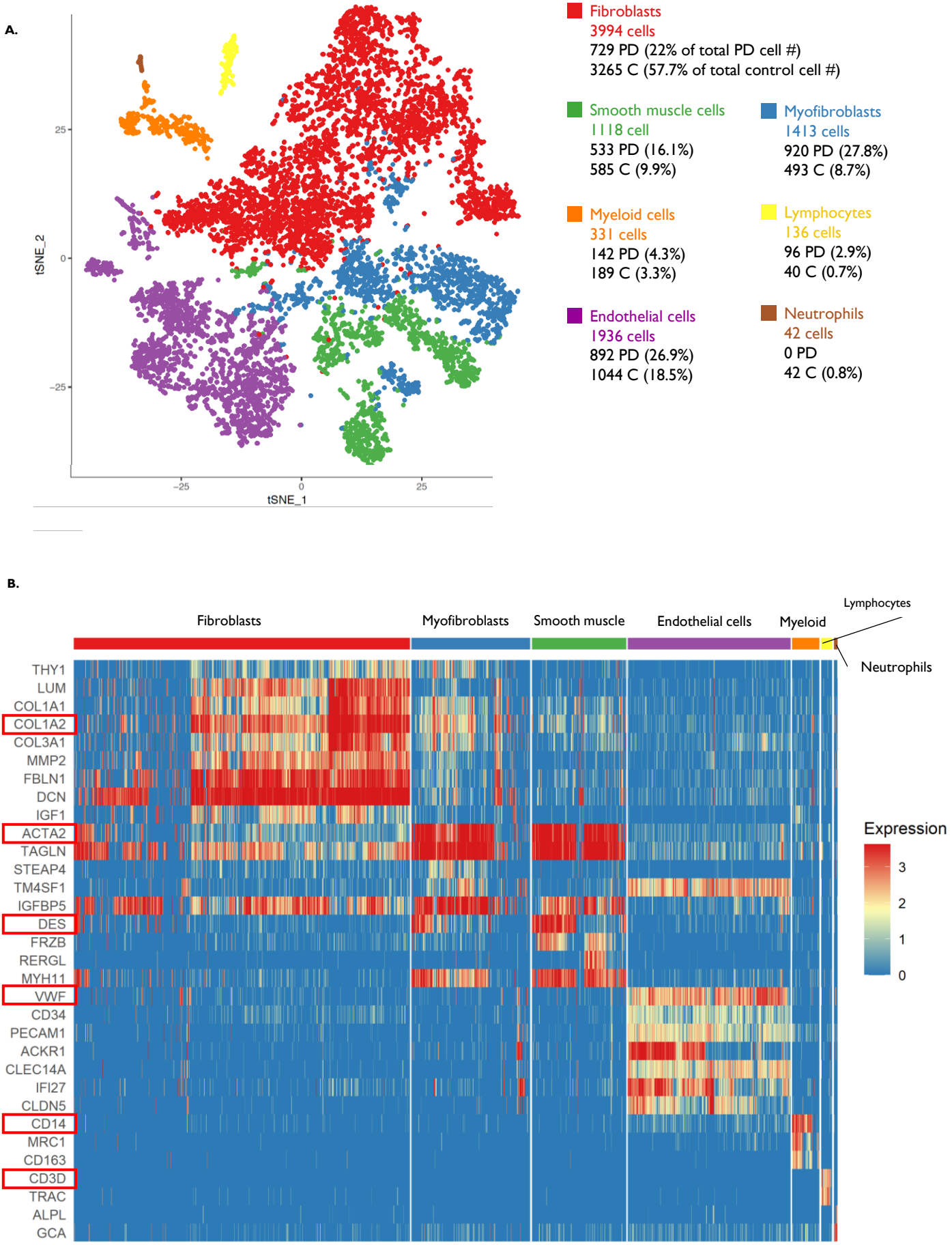
A.
tSNE_2
tSNE_1
25
0
−25
Fibroblasts
3994 cells
729 PD (22% of total PD cell #)
3265 C (57.7% of total control cell #)
Smooth muscle cells
1118 cell
533 PD (16.1%)
585 C (9.9%)
Myofibroblasts
1413 cells
920 PD (27.8%)
493 C (8.7%)
Myeloid cells
331 cells
142 PD (4.3%)
189 C (3.3%)
Lymphocytes
136 cells
96 PD (2.9%)
40 C (0.7%)
Endothelial cells
1936 cells
892 PD (26.9%)
1044 C (18.5%)
Neutrophils
42 cells
0 PD
42 C (0.8%)
B.
Fibroblasts
Myofibroblasts
Smooth muscle
Endothelial cells
Myeloid
Lymphocytes
Neutrophils
THY1
LUM
COL1A1
COL1A2
COL3A1
MMP2
FBLN1
DCN
IGF1
ACTA2
TAGLN
STEAP4
TM4SF1
IGFBP5
DES
FRZB
RERGL
MYH11
VWF
CD34
PECAM1
ACKR1
CLEC14A
IFI27
CLDN5
CD14
MRC1
CD163
CD3D
TRAC
ALPL
GCA
Expression
3
2
1
0

Figure 5

C.

COL1A2

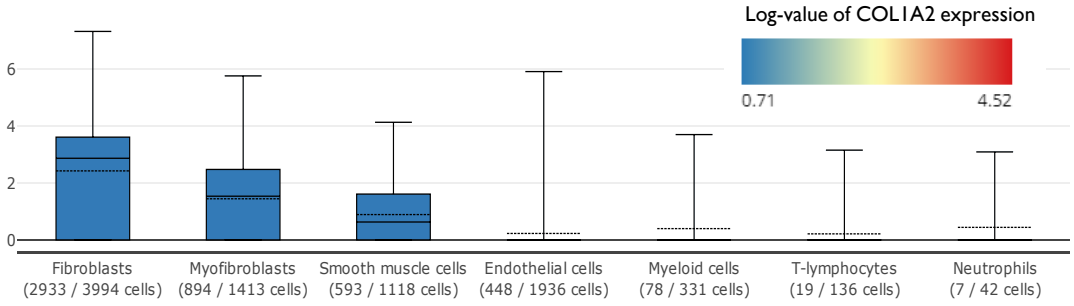

ACTA2

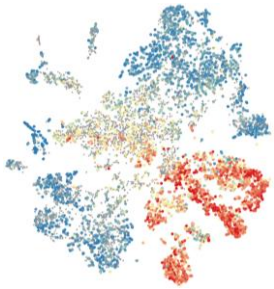

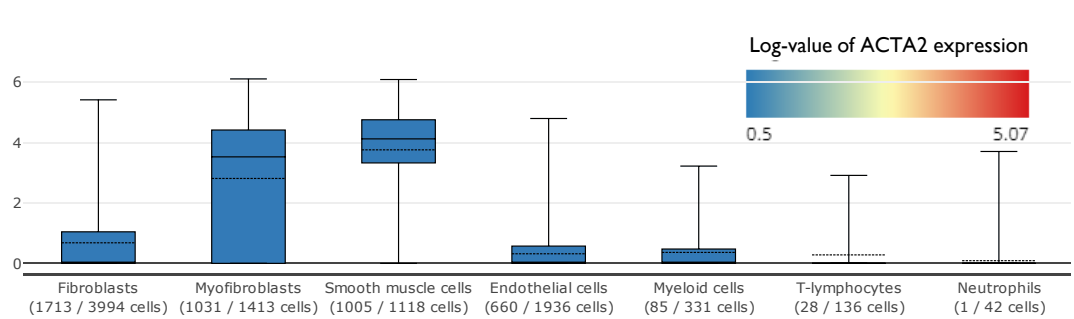

DESMIN

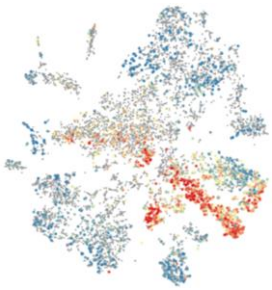

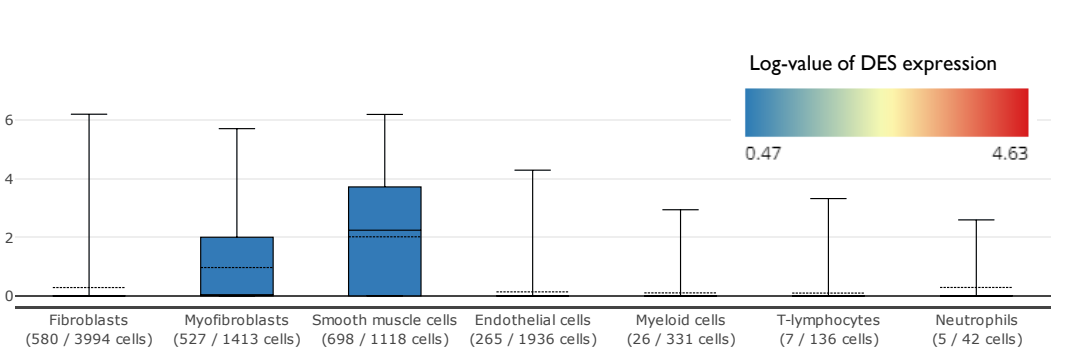

VWF

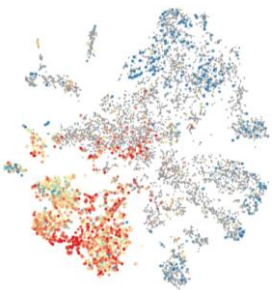

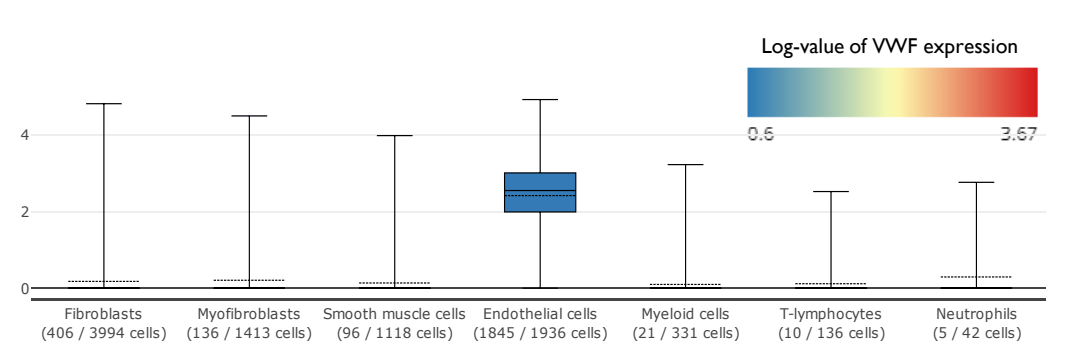

CD14

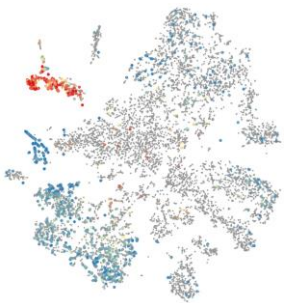

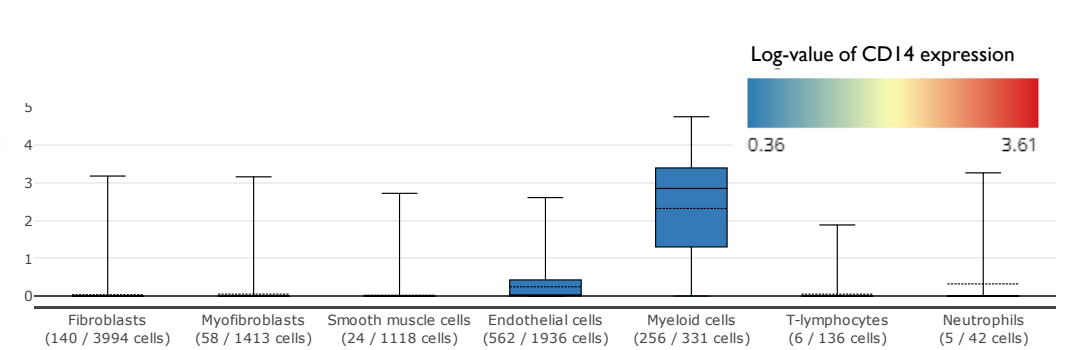

CD3D

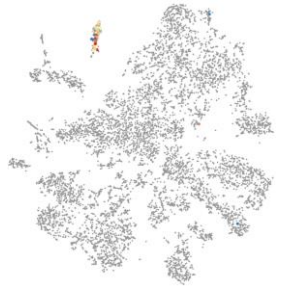

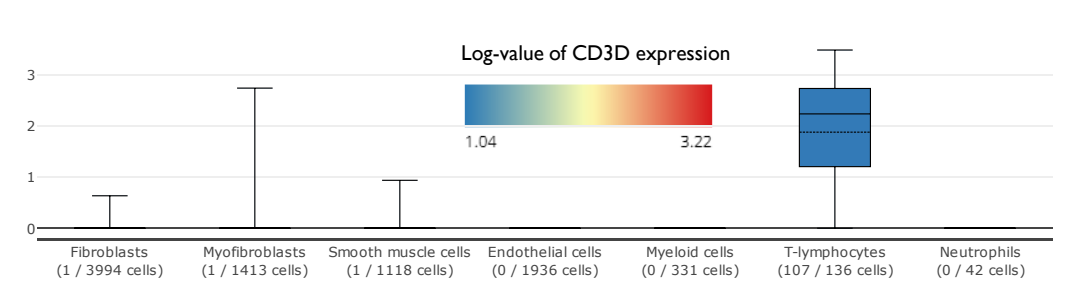

Figure 5

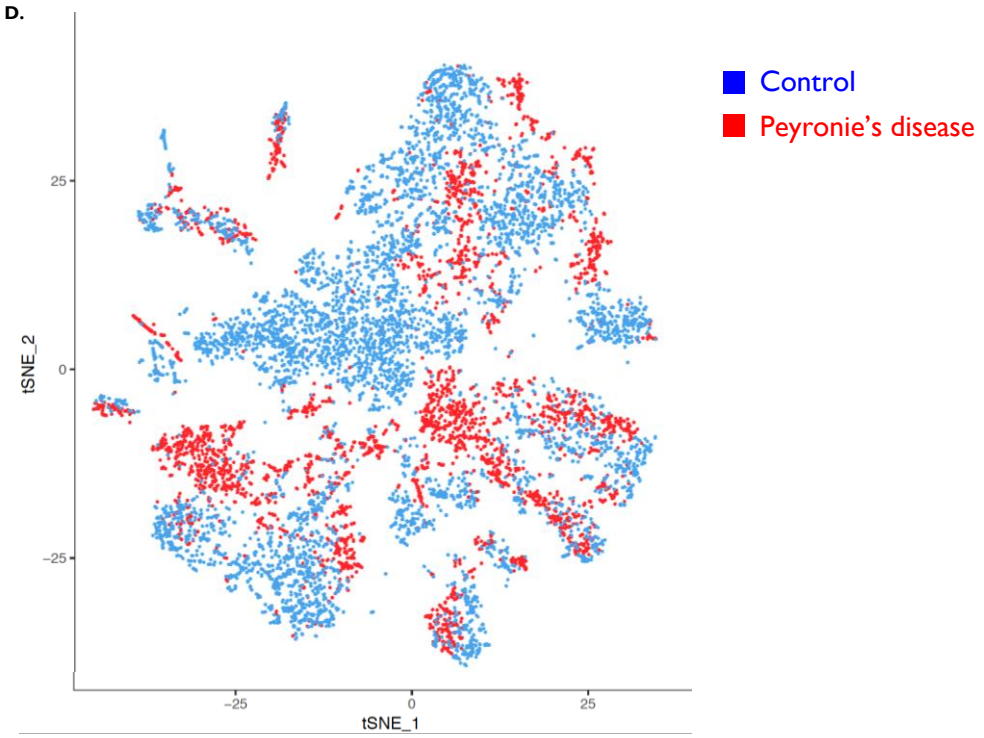
D.
Control
Peyronie's disease
tSNE_2
tSNE_1
25
0
−25
−25
0
25

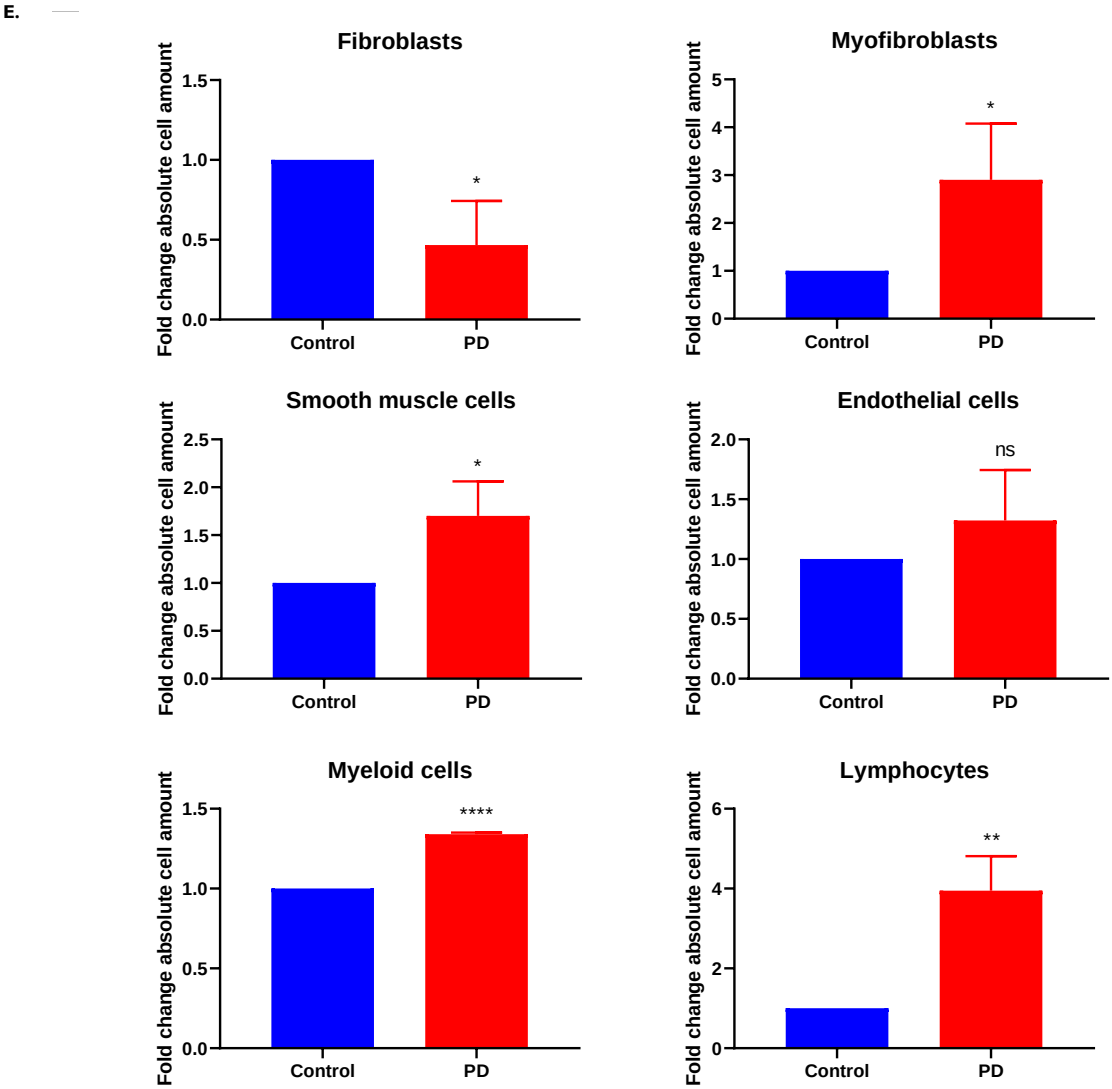
E.
Fibroblasts
Fold change absolute cell amount
1.5
1.0
0.5
0.0
*
Control
PD
Myofibroblasts
Fold change absolute cell amount
5
4
3
2
1
0
*
Control
PD
Smooth muscle cells
Fold change absolute cell amount
2.5
2.0
1.5
1.0
0.5
0.0
*
Control
PD
Endothelial cells
Fold change absolute cell amount
2.0
1.5
1.0
0.5
0.0
ns
Control
PD
Myeloid cells
Fold change absolute cell amount
1.5
1.0
0.5
0.0
****
Control
PD
Lymphocytes
Fold change absolute cell amount
6
4
2
0
**
Control
PD

Figure 5. Overview of the 8970 control and Peyronie's disease cells.

A. tSNE of the 8970 cells profiled. To reduce dimensionality of this dataset, the resulting variably expressed genes were summarized by principle component analysis, and the first 19 principle components further summarized using tSNE dimensionality reduction. Resolution was set for 0.8. Clusters were annotated through unsupervised clustering, manual curation and colored according to their corresponding detailed gene expression (Fig. B). Fibroblasts (red) contained 3994 cells in total, 729 cells in PD (which comprises 22% of the total PD cell population) and 3265 belonging to the control sample (comprising 57.7% of total control cell number). Myofibroblasts (blue) contained 1413 cells in total, 920 cells in PD (which comprises 27.8% of the total PD cell population) and 493 belonging to the control sample (comprising 8.7% of total control cell number). Smooth muscle cells (green) contained 1118 cells in total, 533 cells in PD (which comprises 16.1% of the total PD cell population) and 585 belonging to the control sample (comprising 9.9% of total control cell number). Myeloid cells (orange) contained 331 cells in total, 142 cells in PD (which comprises 4.3% of the total PD cell population) and 189 belonging to the control sample (comprising 3.3% of total control cell number). Lymphocytes (yellow) contained 136 cells in total, 96cells in PD (which comprises 2.9% of the total PD cell population) and 40 belonging to the control sample (comprising 0.7% of total control cell number). Endothelial cells (purple) contained 1936 cells in total, 892 cells in PD (which comprises 26.9% of the total PD cell population) and 1044 belonging to control sample (comprising 18.5% of total control cell number). Neutrophils (brown) contained 42 cells in total, 0 cells in PD and 42 belonging to control sample (comprising 0,8% of total control cell number).

B. Heatmap with gene expression per individual cell (rows are genes, columns are individual cells). Red: fibroblasts (THY1+, LUM+, COL1A1+, COL3A1+, MMP2+, FBLN1+, DCN+), blue: myofibroblasts (presence of fibroblast markers + ACTA2+, TAGLN+, STEAP4+, TM4SF1+, IGFBP5+), green: smooth muscle cells (SMC) (ACTA2+, TAGLN+, IGFBP5+, DES+, FRZB+, RERGL+, MYH11+ and absence of fibroblast markers), endothelial cells (EC) (VWF+, CD34+, PECAM1+, ACKR1+, CLEC14A+, IFI27, CLDN5), myeloid cells (CD14, MRC1, CD163), T-lymphocytes (CD3D, TRAC) and neutrophils (NP) (ALPL, GCA)

C. Gene expression of individual genes was visualised by boxplots. Pseudocolored t-SNE plots for expression of marker genes for different cell types. To the right of each tSNE figure, there is a boxplot annotating the relative fold change expression of that gene per cluster. Red = high expression, blue = low expression, grey = no expression.

D-E. Each cell was color coded according to their origin tissue (blue = control, red = Peyronie's disease). Bar graph showing the fold change in absolute number of fibroblasts (FB), myofibroblasts (MFB), smooth muscle cells (SMC), endothelial cells (EC), myeloid cells and T-lymphocytes. This graph shows a significant decrease in fibroblasts (50% decrease) ($p<0.05$), 1.7-fold increase in SMC ($p<0.05$), 1.3-fold increase in EC (ns) and 2,9-fold increase in MFB ($p<0.05$) for PD samples compared to control. Moreover, myeloid cells were 1.34-fold increased ($p<0.0001$) and lymphocytes were 3.9-fold increased ($p<0.01$). Data visualization and bar graphs were made using Graphpad Prism v8.0.1

Figure 6. Subclustering myeloid cells

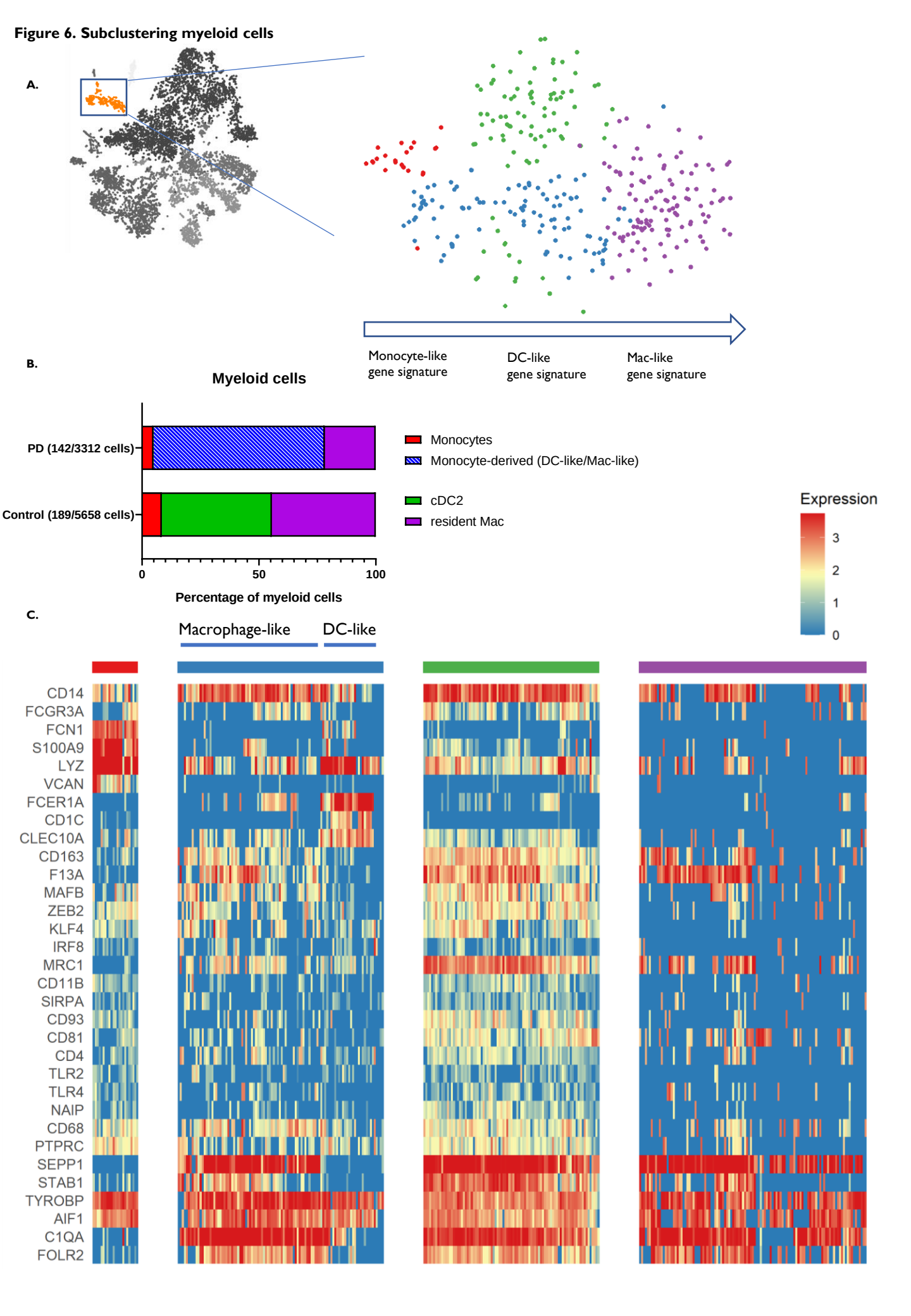

Figure 6. Subclustering myeloid cells

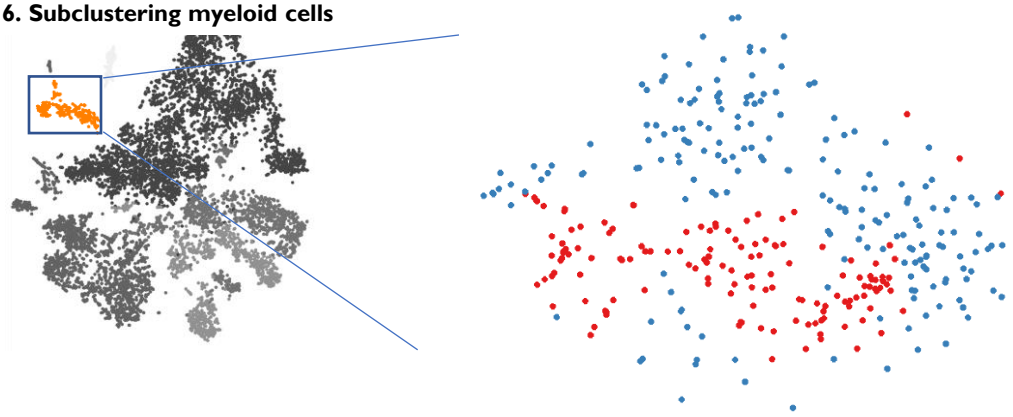

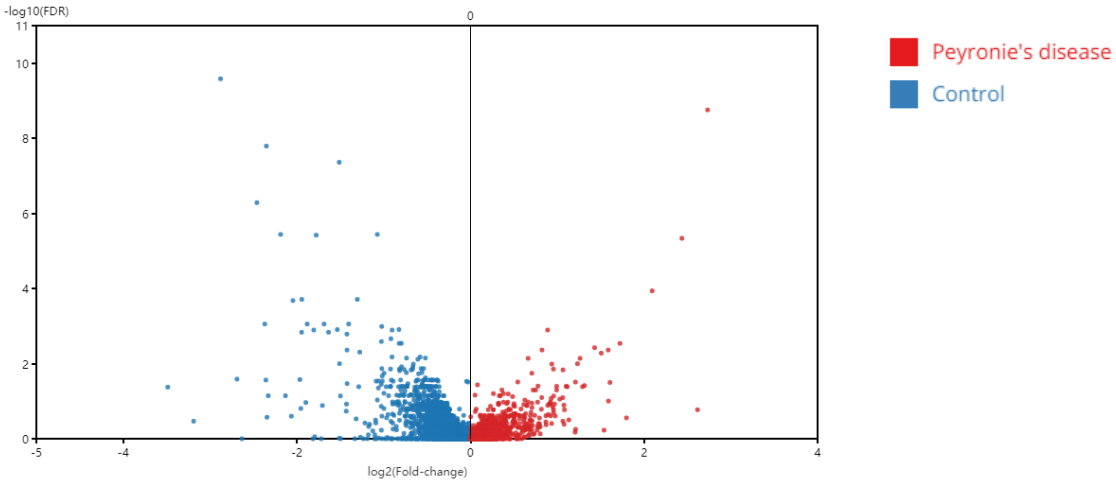

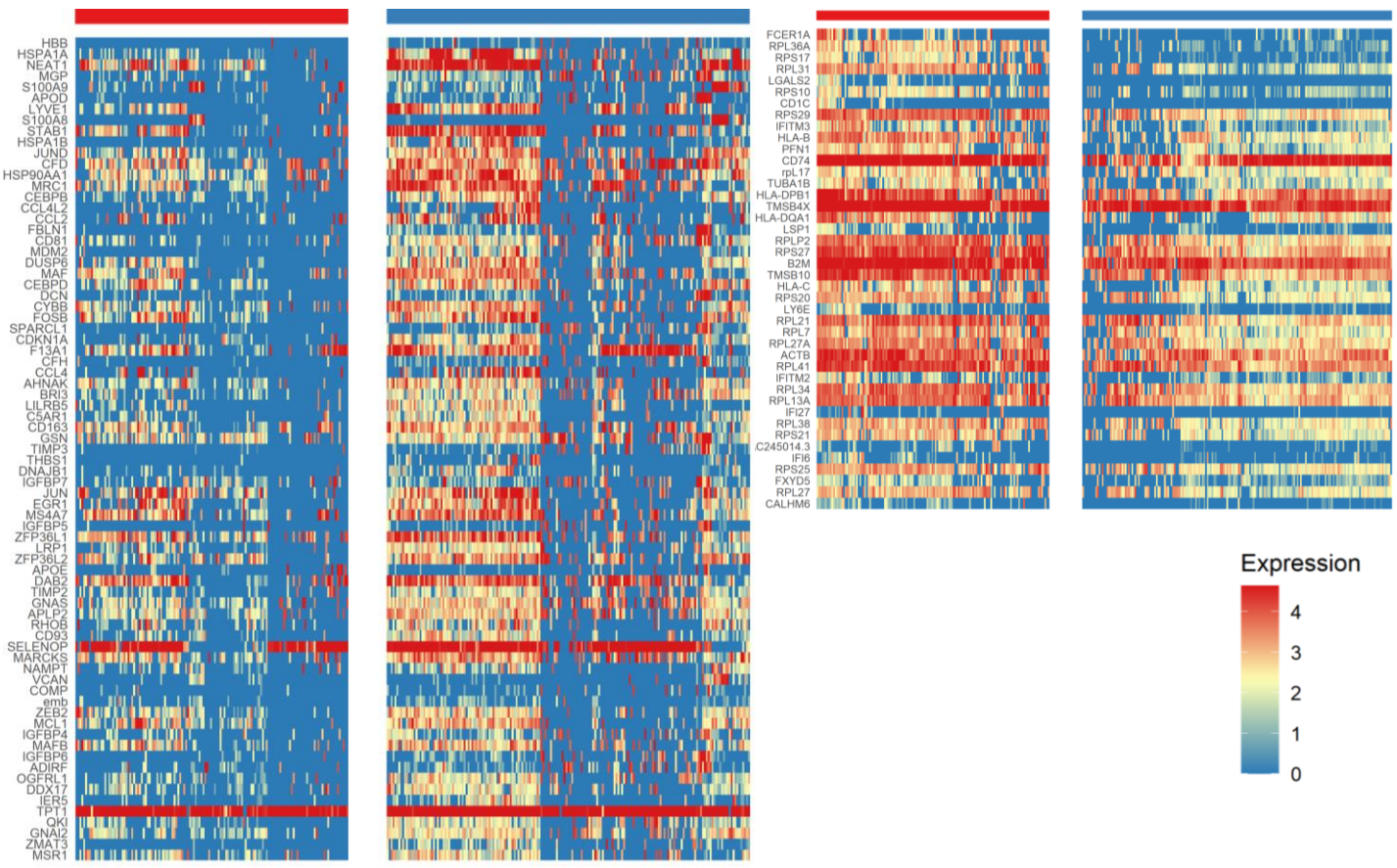

Fig. 6 Subclustering of myeloid cell cluster

A. *Myeloid cells are further subclustered using BioTuring unsupervised subclustering and manual curation. Myeloid cells lie on a spectrum of monocyte, DC-like and macrophage-like gene expression.*

B. *Bar graph showing the relative distribution of subclustered cells within the myeloid cell cluster. PD myeloid cells (n=142/3312) consist of 5% monocytes (red), 73% monocyte-derived cells (either DC-like or Mac-like) (blue) and 22% of resident macrophages (purple). Control myeloid cells (n=189/5658) consist of 8.5% monocytes, 47% classical dendritic cells type 2 (green) and 44.5% resident macrophages.*

C. *Expression heatmap showing gene expression per subcluster. CD14, FCN1, S100A9, LYZ, VCAN are considered monocyte-related genes. FCER1A, CD1C, CLEC10A, ZEB2, KLF4, IRF8, CD11b, SIRPA, CD93, CD81, CD4, TLR2/4, NAIP, MRC1 are considered dendritic cell-related genes. CD163, F13A, MAFB, CD68, SEPP1, STAB1, TYROBP, AIF1, C1QA, FOLR2 are considered macrophage-related genes (predominantly M2)*

D. Each cell was color coded according to their origin tissue (blue = control, red = Peyronie's disease).

E. Volcano plot of differentially expressed genes (also shown in table 1 and 2). X-axis contains log2 fold change (positive (red) = increased gene expression of PD compared to control, negative (blue) = decreased gene expression of PD compared to control). Y-axis contains –log10 false discovery rate p-value.

F. Heatmap of every gene up- or downregulated (resp. right and left heatmap) with a fold change of >1.5 (cfr. Table 1-2)

Figure 7. Subclustering T-lymphocytes

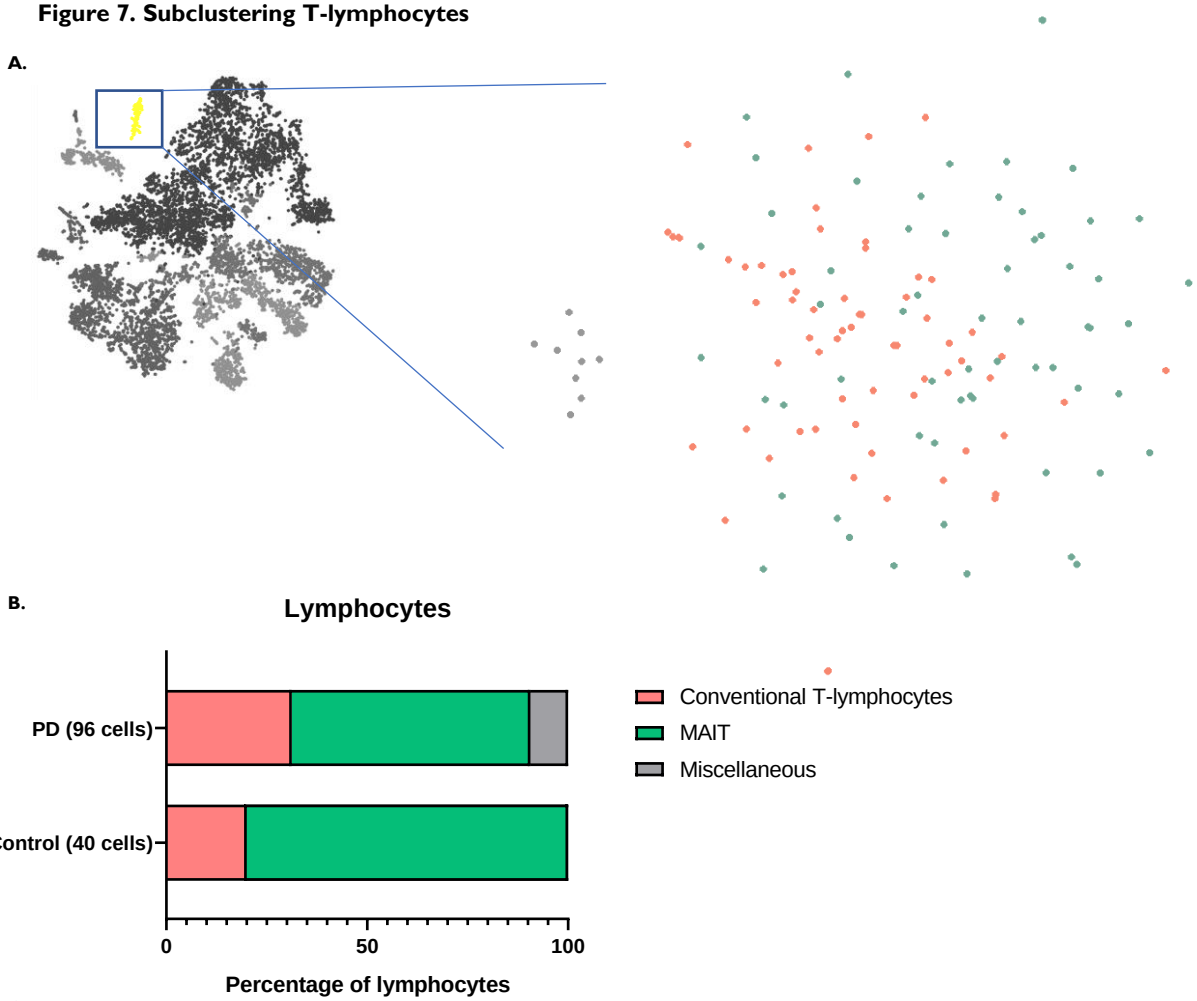

Figure 7.

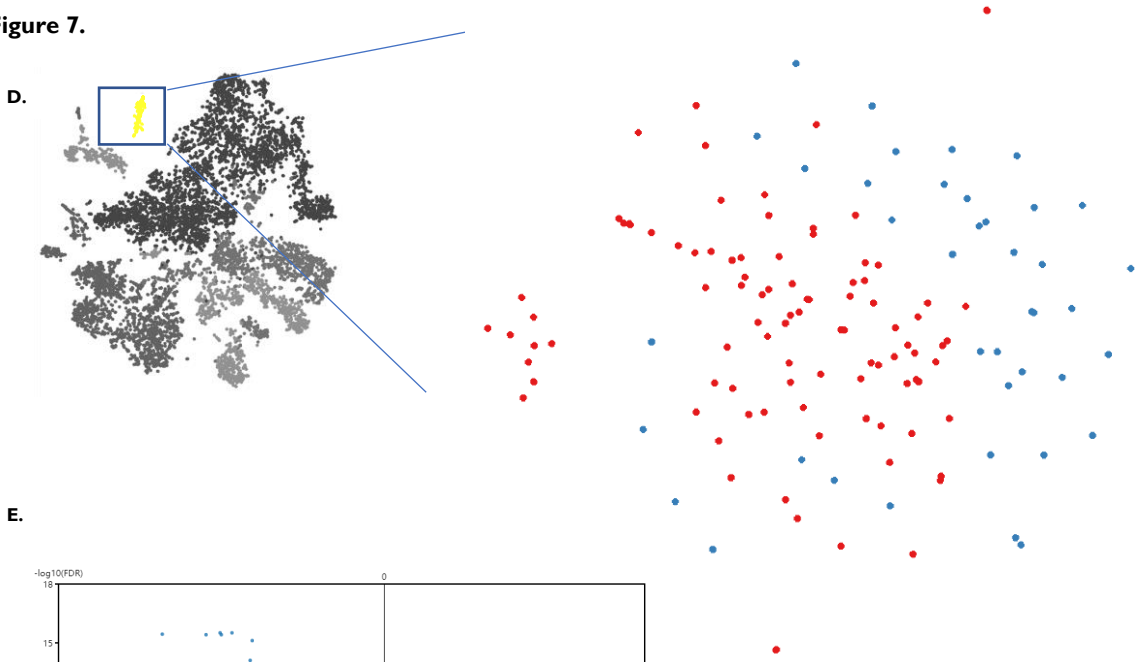
D.

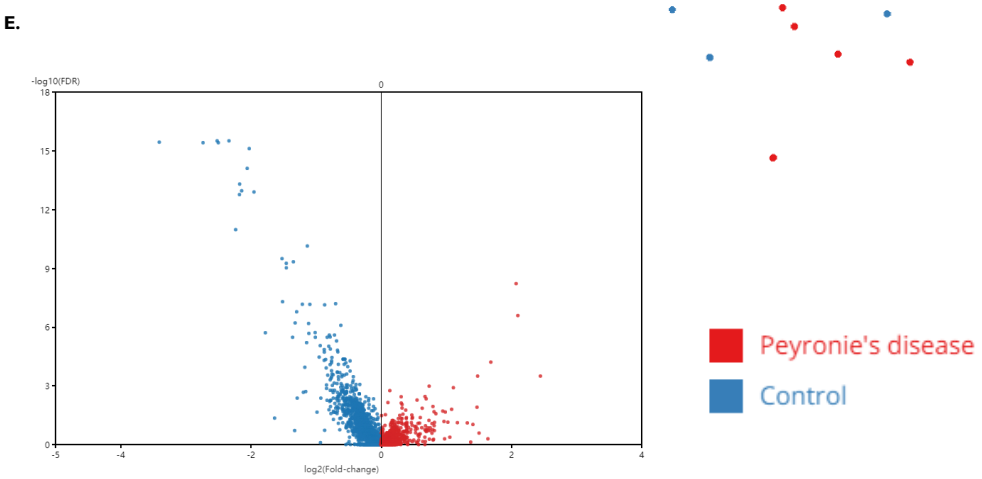
E.
-log10(FDR)
log2(Fold-change)
Peyronie's disease
Control

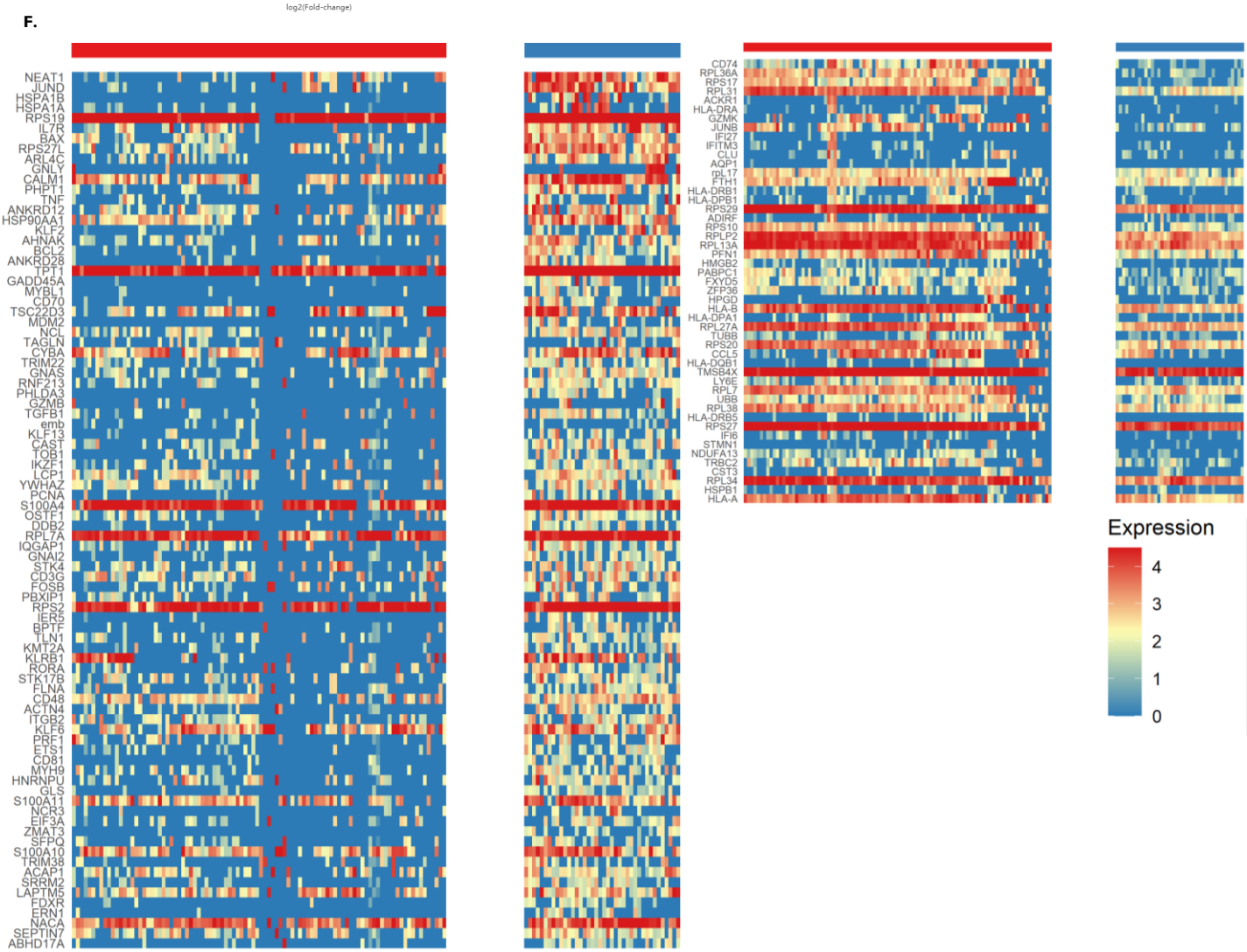
F.
NEAT1
JUND
HSPA1B
HSPA1A
RPS19
IL7R
BAX
RPS27L
ARL4C
GNLY
CALM1
PHPT1
TNF
ANKRD12
HSP90AA1
KLF2
AHNAK
BCL2
ANKRD28
TPT1
GADD45A
MYBL1
CD70
TSC22D3
MDM2
NCL
TAGLN
CYBA
TRIM22
GNAS
RNF213
PHLDA3
GZMB
TGFB1
emb
KLF13
CAST
TOB1
IKZF1
LCP1
YWHAZ
PCNA
S100A4
OSTF1
DDB2
RPL7A
IQGAP1
GNAI2
STK4
CD3G
FOSB
PBXIP1
RPS2
IER5
EPTE
TLN1
KMT2A
KLRB1
RORA
STK17B
FLNA
CD48
ACTN4
ITGB2
KLF6
PRF1
ETS1
CD81
MYH9
HNRNPU
GLS
S100A11
NCR3
EIF3A
ZMAT3
SFPQ
S100A10
TRIM38
ACAP1
SRRM2
LAPTM5
FDXR
ERN1
NACA
SEPTIN7
ABHD17A
CD74
RPL36A
RPS17
RPL31
ACKR1
HLA-DRA
GZMK
JUNB
IFI27
IFITM3
CLU
AQP1
rpL17
FTH1
HLA-DRB1
HLA-DPB1
RPS29
ADIRF
RPS10
RPLP2
RPL13A
PFN1
HMGB2
PABPC1
FXYD5
ZFP36
HPGD
HLA-B
HLA-DPA1
RPL27A
TUBB
RPS20
CCL5
HLA-DQB1
TMSB4X
LY6E
RPL7
UBB
RPL38
HLA-DRB5
RPS27
IFI6
STMN1
NDUFA13
TRBC2
CST3
RPL34
HSPB1
HLA-A
Expression
4
3
2
1
0

Fig. 7 Subclustering of myeloid cell cluster

A. *Lymphoid cells are further subclustered using BioTuring unsupervised subclustering and manual curation.*

B. *Bar graph showing the relative distribution of subclustered cells within the lymphoid cell cluster. PD lymphoid cells (n=96/3312) consist of 31.2% conventional T-lymphocytes (CD4+ or CD8+) (pink) and 59.4% non-conventional mucosal-associated invariant T-lymphocytes (MAIT) (light green) and 9.4% miscellaneous (B-lymphocytes, NK cells, basophils) (grey). Control lymphoid* ***cells (n=40/5658) consist of 20%*** *conventional T-lymphocytes (CD4+ or CD8+) and 80% non-conventional mucosal-associated invariant T-lymphocytes (MAIT).*

C. *Expression heatmap showing gene expression per subcluster. TRAC, CD3D and CD3E are canonical T-cell markers. We can distinguish CD4+, CD8+ and few double negative conventional T and non-conventional MAIT. KLRB1, CD127, CCR6 and CXCR6 are MAIT –associated genes, while GZMA, GZMK, GZMM, CCL4, CCL5, CXCR3, PTPRC, negative for CD62L and CCR7 are frequently associated with cytotoxic T-lymphocytes*

D. *Each cell was color coded according to their origin tissue (blue = control, red = Peyronie's disease).*

E. *Volcano plot of differentially expressed genes (also shown in table 1 and 2). X-axis contains log2 fold change (positive (red) = increased gene expression of PD compared to control, negative (blue) = decreased gene expression of PD compared to control). Y-axis contains –log10 false discovery rate p-value.*

F. *Heatmap of every gene up- or downregulated (resp. right and left heatmap) with a fold change of >1.5 (cfr. Table 1-2)*

Supplementary table 1. Differential gene expression PD vs control myeloid cells (upregulated). Highlighted in yellow are disease-relevant genes. Annotated in red are disease-relevant genes that, individually, do not reach FDR-corrected statistical significance.

Gene symbol	Log2 fold change	-Log10 false discovery rate	Percentage 1 (present in PD myeloid cells)	Percentage 2 (present in control myeloid cells)
FCER1A	2.277	4.84149	35.91549	19.04762
RPL36A	2.147	24.33653	88.73239	40.74074
RPS17	2.003	20.46146	70.42254	22.22222
RPL31	1.676	10.80639	90.14085	71.95767
LGALS2	1.28	9.00661	28.87324	1.5873
RPS10	1.181	8.0911	82.39437	55.55556
CD1C	1.155	3.26317	16.90141	3.7037
RPS29	1.144	4.21843	96.47887	90.47619
IFITM3	1.121	3.90173	71.83099	55.55556
HLA-B	1.1	3.30843	89.43662	77.77778
PFN1	1.073	2.97685	83.09859	66.66667
CD74	1.053	5.27391	98.59155	96.8254
RPL17	1.05	8.69572	59.85915	24.33862
TUBA1B	1.027	1.28134	78.16901	70.89947
HLA-DPB1	0.978	2.51798	96.47887	92.06349
TMSB4X	0.975	3.30548	100	99.4709
HLA-DQA1	0.962	1.70257	76.05634	64.02116
LSP1	0.953	3.0264	41.5493	23.80952
RPLP2	0.918	3.80129	93.66197	90.47619
RPS27	0.896	3.4989	97.1831	97.3545
B2M	0.884	3.17139	98.59155	98.4127
TMSB10	0.84	2.44149	94.3662	93.12169
HLA-C	0.838	1.65747	76.05634	68.25397
RPS20	0.794	2.89207	92.25352	83.59788
LY6E	0.78	3.29848	38.02817	17.98942
RPL21	0.775	2.79868	95.07042	92.59259
RPL7	0.769	2.38776	92.25352	85.18519
RPL27A	0.742	2.69161	90.14085	91.53439
ACTB	0.74	2.87609	97.88732	92.06349
RPL41	0.735	2.10969	99.29577	96.2963
IFITM2	0.721	1.02682	59.85915	49.73545
RPL34	0.702	2.62117	91.5493	92.06349
RPL13A	0.671	1.66659	97.1831	94.70899
IFI27	0.662	3.76812	17.60563	3.1746
RPL38	0.656	3.98666	92.95775	82.01058
RPS21	0.655	2.39762	86.61972	79.89418
AC245014.3	0.643	2.68133	27.46479	11.64021
IFI6	0.636	3.67346	30.98592	11.64021
RPS25	0.627	1.63671	92.95775	86.77249
FXYD5	0.619	1.9403	58.4507	49.73545
RPL27	0.613	1.14849	86.61972	81.48148
CALHM6	0.601	6.73388	39.43662	10.05291

Supplementary table 2. Differential gene expression PD vs control myeloid cells (downregulated). Highlighted in yellow are disease-relevant genes. Annotated in red are disease-relevant genes that, individually, do not reach FDR-corrected statistical significance.

Gene symbol	Log2 fold change	Log10 false discovery rate	Percentage 1 (present in PD myeloid cells)	Percentage 2 (present in control myeloid cells)
HBB	-4.039	5.63596	0.70423	17.98942
HSPA1A	-3.024	13.35107	25.35211	65.60847
NEAT1	-2.501	18.37952	55.6338	65.07937
MGP	-2.342	10.31007	18.30986	57.14286
S100A9	-2.122	1.71901	21.83099	37.56614
APOD	-2.019	4.89435	7.74648	30.15873
LYVE1	-1.97	10.63185	27.46479	61.90476
S100A8	-1.945	0.23225	8.4507	10.58201
STAB1	-1.925	11.9164	45.77465	67.72487
HSPA1B	-1.896	11.54821	4.22535	40.74074
JUND	-1.88	11.9286	41.5493	69.84127
CFD	-1.816	9.09042	57.74648	80.42328
HSP90AA1	-1.814	10.29011	59.15493	75.13228
MRC1	-1.787	12.07052	51.40845	69.31217
CEBPB	-1.719	12.25581	24.64789	59.25926
CCL4L2	-1.69	4.13133	7.74648	26.45503
CCL2	-1.678	4.55772	25.35211	48.14815
FBLN1	-1.622	11.583	2.11268	37.56614
CD81	-1.598	14.99919	26.05634	71.42857
MDM2	-1.543	20.02241	2.8169	54.49735
DUSP6	-1.537	10.04784	31.69014	57.67196
MAF	-1.495	9.54381	42.25352	65.07937
CEBPD	-1.457	6.81017	42.25352	63.49206
DCN	-1.436	4.08347	11.26761	32.27513
CYBB	-1.407	10.0733	50	68.25397
FOSB	-1.406	5.21758	46.47887	54.49735
SPARCL1	-1.395	9.02156	5.6338	38.62434
CDKN1A	-1.392	12.29157	19.71831	57.67196
F13A1	-1.368	5.8046	52.8169	75.13228
CFH	-1.354	8.30442	4.22535	34.39153
CCL4	-1.347	3.20619	15.49296	33.86243
AHNAK	-1.287	10.17654	45.77465	68.78307
BRI3	-1.282	10.89023	28.16901	68.25397
LILRB5	-1.243	7.72342	19.71831	48.67725
C5AR1	-1.242	8.54564	19.71831	52.91005
CD163	-1.24	10.24846	52.8169	69.31217
GSN	-1.237	2.61667	57.04225	77.24868
TIMP3	-1.236	6.42899	4.22535	29.10053
THBS1	-1.236	6.16984	0.70423	19.57672
DNAJB1	-1.233	7.13978	12.67606	37.56614
IGFBP7	-1.218	0.49321	35.21127	44.97354
JUN	-1.206	3.77697	52.8169	59.78836
EGR1	-1.201	5.6758	33.09859	61.37566

MS4A7	-1.199	6.61054	56.33803	68.25397
IGFBP5	-1.195	5.21758	3.52113	22.75132
ZFP36L1	-1.191	4.35198	64.78873	69.31217
LRP1	-1.182	11.47556	27.46479	62.43386
ZFP36L2	-1.18	4.45607	47.88732	70.89947
APOE	-1.18	0.12521	11.97183	10.58201
DAB2	-1.179	5.64854	57.04225	78.30688
TIMP2	-1.172	12.13576	25.35211	66.13757
GNAS	-1.172	10.09839	50	82.01058
APLP2	-1.166	10.7742	53.52113	73.01587
RHOB	-1.163	3.90261	27.46479	46.03175
CD93	-1.157	8.69572	22.53521	55.55556
SELENOP	-1.142	4.5687	72.53521	85.18519
MARCKS	-1.13	6.77407	54.22535	77.24868
NAMPT	-1.123	4.6858	26.76056	44.97354
VCAN	-1.114	0.70461	9.85915	15.34392
COMP	-1.099	3.00079	4.22535	16.93122
EMB	-1.096	10.13102	26.76056	59.78836
ZEB2	-1.09	8.05106	45.77465	62.43386
MCL1	-1.086	5.9943	47.88732	58.73016
IGFBP4	-1.086	5.88917	16.90141	45.50265
MAFB	-1.084	5.45777	44.3662	60.84656
IGFBP6	-1.082	6.48275	6.33803	33.33333
ADIRF	-1.078	3.50583	16.90141	38.09524
OGFRL1	-1.075	9.48187	27.46479	63.49206
DDX17	-1.072	11.91901	35.21127	59.78836
IER5	-1.068	6.26849	10.56338	37.56614
TPT1	-1.066	5.20623	97.88732	98.9418
QKI	-1.048	11.50212	30.28169	66.13757
GNAI2	-1.009	7.00495	42.95775	73.01587
ZMAT3	-1.006	10.7324	3.52113	38.09524
MSR1	-1.001	8.0911	40.84507	55.02646

Supplementary table 3. Differential gene expression PD vs control lymphoid cells (upregulated). Highlighted in yellow are disease-relevant genes. Annotated in red are disease-relevant genes that, individually, do not reach FDR-corrected statistical significance.

Gene symbol	Log2 fold change	-Log10 false discovery rate	Percentage 1 (present in PD lymphoid cells)	Percentage 2 (present in control lymphoid cells)
CD74	2.445	3.49629	70.83333	32.5
RPL36A	2.099	6.58484	86.45833	50
RPS17	2.072	8.21709	88.54167	32.5
RPL31	1.684	4.2074	96.875	95
ACKR1	1.639	0.29196	11.45833	5
HLA-DRA	1.503	0.58449	26.04167	12.5
GZMK	1.481	3.49556	45.83333	5
JUNB	1.471	1.90691	64.58333	55
IFI27	1.409	1.02571	10.41667	0
IFITM3	1.375	0.12589	20.83333	15
CLU	1.322	1.10343	26.04167	32.5
AQP1	1.17	1.11572	11.45833	0
RPL17	1.109	2.904	71.875	35
FTH1	1.082	1.7992	90.625	100
HLA-DRB1	1.054	0.37462	34.375	20
HLA-DPB1	1.024	1.14176	40.625	15
RPS29	0.985	1.66118	98.95833	100
ADIRF	0.974	0.29196	17.70833	27.5
RPS10	0.965	1.17745	83.33333	80
RPLP2	0.946	1.70825	97.91667	100
RPL13A	0.84	1.57365	96.875	100
PFN1	0.819	1.13183	89.58333	92.5
HMGB2	0.817	0.7128	34.375	17.5
PABPC1	0.814	0.96367	69.79167	65
FXYD5	0.812	1.67447	70.83333	62.5
ZFP36	0.805	0.26694	56.25	50
HPGD	0.797	0.22723	12.5	20
HLA-B	0.795	1.94175	91.66667	100
HLA-DPA1	0.791	0.7553	36.45833	22.5
RPL27A	0.781	1.07187	97.91667	100
TUBB	0.78	0.57944	44.79167	40
RPS20	0.751	0.71115	92.70833	97.5
CCL5	0.741	0.2721	64.58333	47.5
HLA-DQB1	0.737	2.98115	28.125	0
TMSB4X	0.734	1.23371	98.95833	97.5
LY6E	0.72	0.7136	63.54167	40
RPL7	0.716	0.85397	91.66667	100
UBB	0.697	0.75093	78.125	72.5
RPL38	0.695	0.6628	95.83333	97.5
HLA-DRB5	0.691	2.33304	22.91667	0

RPS27	0.683	0.69971	97.91667	100
IFI6	0.68	0.95691	31.25	12.5
STMN1	0.678	0.15674	12.5	7.5
NDUFA13	0.673	2.44967	63.54167	27.5
TRBC2	0.672	0.76212	66.66667	57.5
CST3	0.672	0	20.83333	22.5
RPL34	0.671	0.37675	98.95833	100
HSPB1	0.638	0.15674	27.08333	20
HLA-A	0.63	1.85416	91.66667	97.5

Supplementary table 4. Differential gene expression PD vs control lymphoid cells (downregulated). Highlighted in yellow are disease-relevant genes. Annotated in red are disease-relevant genes that, individually, do not reach FDR-corrected statistical significance.

Gene symbol	Log2 fold change	-Log10 false discovery rate	Percentage 1 (present in PD lymphoid cells)	Percentage 2 (present in control lymphoid cells)
NEAT1	-2.234	10.97329	29.16667	92.5
JUND	-2.142	12.95706	22.91667	95
HSPA1B	-1.778	5.70664	1.04167	47.5
HSPA1A	-1.636	1.34846	15.625	40
RPS19	-1.522	9.49338	95.83333	100
IL7R	-1.514	7.29457	32.29167	92.5
BAX	-1.457	9.25373	36.45833	90
RPS27L	-1.456	9.02334	47.91667	95
ARL4C	-1.36	5.4766	25	77.5
GNLY	-1.328	0.7136	5.20833	17.5
CALM1	-1.321	6.20876	71.875	97.5
PHPT1	-1.297	6.77918	25	80
TNF	-1.289	2.37111	10.41667	42.5
ANKRD12	-1.195	2.66985	50	82.5
HSP90AA1	-1.172	3.94531	60.41667	92.5
KLF2	-1.158	2.70331	10.41667	45
AHNAK	-1.144	5.20205	38.54167	80
BCL2	-1.134	10.13778	8.33333	77.5
ANKRD28	-1.114	6.18106	14.58333	70
TPT1	-1.11	5.67355	94.79167	100
GADD45A	-1.095	7.15657	4.16667	60
MYBL1	-1.014	5.71636	5.20833	55
CD70	-1.011	5.4766	3.125	50
TSC22D3	-0.985	1.65396	61.45833	77.5
MDM2	-0.952	4.46375	2.08333	42.5
NCL	-0.936	5.05014	42.70833	85
TAGLN	-0.932	0.0981	21.875	27.5
CYBA	-0.926	2.37101	76.04167	87.5
TRIM22	-0.875	4.30004	26.04167	72.5
GNAS	-0.874	4.8489	34.375	77.5

RNF213	-0.873	4.71935	29.16667	80
PHLDA3	-0.868	7.13323	0	52.5
GZMB	-0.868	0.72627	8.33333	22.5
TGFB1	-0.852	4.34357	20.83333	70
EMB	-0.844	3.91181	30.20833	72.5
KLF13	-0.839	3.0422	10.41667	47.5
CAST	-0.838	2.86514	31.25	72.5
TOB1	-0.831	2.26009	16.66667	50
IKZF1	-0.829	5.4766	25	80
LCP1	-0.821	3.54138	40.625	85
YWHAZ	-0.801	1.77614	45.83333	77.5
PCNA	-0.796	5.59045	7.29167	57.5
S100A4	-0.79	2.20158	90.625	100
OSTF1	-0.784	4.08032	32.29167	75
DDB2	-0.783	5.49409	9.375	60
RPL7A	-0.783	3.30471	90.625	100
IQGAP1	-0.782	2.7684	29.16667	70
GNAI2	-0.78	4.87691	13.54167	62.5
STK4	-0.78	2.25493	39.58333	72.5
CD3G	-0.778	1.93964	43.75	77.5
FOSB	-0.773	2.25493	29.16667	62.5
PBXIP1	-0.771	1.5809	26.04167	55
RPS2	-0.768	3.38538	89.58333	100
IER5	-0.763	4.1721	3.125	42.5
BPTF	-0.762	3.45931	10.41667	50
TLN1	-0.761	4.27191	26.04167	75
KMT2A	-0.756	4.44391	11.45833	57.5
KLRB1	-0.754	3.60215	30.20833	77.5
RORA	-0.75	3.01944	22.91667	62.5
STK17B	-0.748	2.76622	34.375	75
FLNA	-0.737	3.56367	22.91667	70
CD48	-0.737	2.6576	63.54167	95
ACTN4	-0.735	2.37111	19.79167	55
ITGB2	-0.733	1.69474	42.70833	70
KLF6	-0.733	1.28139	73.95833	95
PRF1	-0.726	1.6403	27.08333	52.5
ETS1	-0.721	3.1406	18.75	60
CD81	-0.717	5.59045	7.29167	57.5
MYH9	-0.716	2.7684	23.95833	62.5
HNRNPU	-0.712	2.09948	34.375	70
GLS	-0.699	7.19063	7.29167	65
S100A11	-0.698	1.85416	70.83333	90
NCR3	-0.698	1.64342	8.33333	32.5
EIF3A	-0.689	2.34481	27.08333	60
ZMAT3	-0.685	5.28883	1.04167	45
SFPQ	-0.684	1.94175	20.83333	50
S100A10	-0.678	3.11382	71.875	92.5
TRIM38	-0.678	1.57931	17.70833	45
ACAP1	-0.674	3.70328	46.875	90
SRRM2	-0.672	2.66138	19.79167	60

LAPTM5	-0.672	1.70385	67.70833	92.5
FDXR	-0.671	4.81485	5.20833	50
ERN1	-0.671	3.68053	2.08333	37.5
NACA	-0.67	2.43956	85.41667	95
SEPTIN7	-0.67	2.231	52.08333	87.5
ABHD17A	-0.665	4.72839	10.41667	57.5